GEOLOGICA CARPATHICA, FEBRUARY 2023, 74, 1, 23–39 https://doi.org/10.31577/GeolCarp.2023.05

Geochemistry and tectonic significance of metamorphosed mafic ophiolitic rocks in the upper high-grade basement unit of the eastern Rhodope Massif (Bulgaria–Greece)

NIKOLAY BONEV[1,✉], ZORNITSA DOTSEVA[1] and PETYO FILIPOV[2]

[1]Department of Geology, Paleontology and Fossil Fuels, Sofia University "St. Kliment Ohridski", 1504 Sofia, Bulgaria; ✉niki@gea.uni-sofia.bg
[2]Department of Geochemistry and Petrology, Geological Institute, Bulgarian Academy of Sciences, 1113 Sofia, Bulgaria

(Manuscript received June 22, 2022; accepted in revised form January 30, 2023; Associate Editor: Igor Broska)

Abstract: Metamorphosed mafic ophiolitic rocks in the metamorphic section of the eastern Rhodope Massif in Bulgaria and Greece are important for understanding the oceanic lithosphere fragments, which have been involved in Alpine tectonic–metamorphic processes. Petrography and mineral compositions of the meta-mafic rocks (mostly gabbro–basalt to minor diorite–andesite) point to main amphibolite-facies overprint, which strongly obliterated the primary textures, and the original igneous grain-sizes are partly preserved only of the plagioclase. The meta-mafic rocks are classified as low-K and low- to high-Ti tholeiitic affinity igneous protoliths of basaltic to andesitic compositions, in which high-Ti and low-Ti groups are identified on the basis of Ti concentrations. They also differ with respect to trace element and REE characteristics. A complex chemistry of high-Ti group indicates an origin primarily from MORB mantle source, subsequently modified by subduction-zone derived LILE- and REE-enriched melts and contribution of HFSE-enriched component that produce the oceanic island tholeiites. The low-Ti group displays IAT affinity, with clearly defined subduction-related component demonstrated by LILE enrichment, HFSE and HREE depletion relative to N-MORB and negative Nb and Ti anomalies, all indicative for an island arc petrogenesis. A single dunite sample studied also displays geochemical characteristics of the low-Ti group meta-mafic rocks. Geochemical diversity of the meta-basic rocks with MORB, transitional MORB/IAT and IAT affinities hints their supra-subduction zone (SSZ) origin in an island arc/back-arc system, with identifiable arc-related and rifting/sea-floor spreading magmatic products represented by the low-Ti and high-Ti groups, respectively. At present, the available Middle-Late Paleozoic/Early Triassic radiometric ages of the meta-mafic rocks protoliths predominate over the Early Paleozoic ages, which suggests that the development of the inferred arc/back-arc system relates mostly to the ocean-floor magmatic evolution of the Paleotethyan realm.

Keywords: meta-mafic ophiolitic rocks, high-grade basement, geochemistry, MOR, SSZ, eastern Rhodope Massif, Bulgaria, Greece

Introduction

The Alpine collisional system of the northern Aegean region is characterized by widespread occurrences of Mesozoic ophiolites (Fig. 1, inset; e.g. Robertson 2002 for review; Papanikolaou 2009), which represent remnants of the oceanic lithosphere that formed during the Late Paleozoic–Mesozoic geodynamic evolution in the Tethys realm (Robertson et al. 1996; Stampfli 2000; Çelik 2002; Parlak et al. 2006; Gartzos et al. 2009; Stampfli & Hochard 2009; Daşçı et al. 2015; Nurlu 2020; Höhn et al. 2022).

The Rhodope Massif constitutes a major tectonic zone of the Alpine system in the northern Aegean region (Fig. 1, inset) and contains widespread mafic-ultramafic meta-ophiolite bodies dispersed within the high-grade metamorphic basement (e.g. Kozhoukharov et al. 1988). These oceanic lithosphere components are generally considered as remnants of the Tethyan ocean floor (Burg et al. 1996; Robertson et al. 1996; Papanikolaou 2009, 2013). The eastern part of the Rhodope Massif exposes mafic and mostly large ultramafic meta-ophiolite bodies. However, their origin is not well understood, with incomplete geochemical signature to constrain more precisely past tectonic environment(s) responsible for the generation of the oceanic crust fragments. Therefore, the details on the geochemistry of meta-ophiolitic rocks are particularly important because they offer a key to assessing the original tectonic setting of formation of the oceanic lithosphere components involved during the Mesozoic geodynamic evolution in this part of the Tethyan domain.

This paper focuses on the metamorphosed mafic (mostly gabbro/basalt) ophiolitic rocks from the eastern part of the Rhodope Massif in southern Bulgaria and northern Greece, providing new data on their geochemical characteristics and tectonic setting. The aim of this study is to extend the knowledge of the geochemical signature of meta-mafic rocks in the high-grade basement and to contribute to a better understanding of the tectonic setting for their origin, which will have implications for the Tethyan geodynamic evolution of the region.

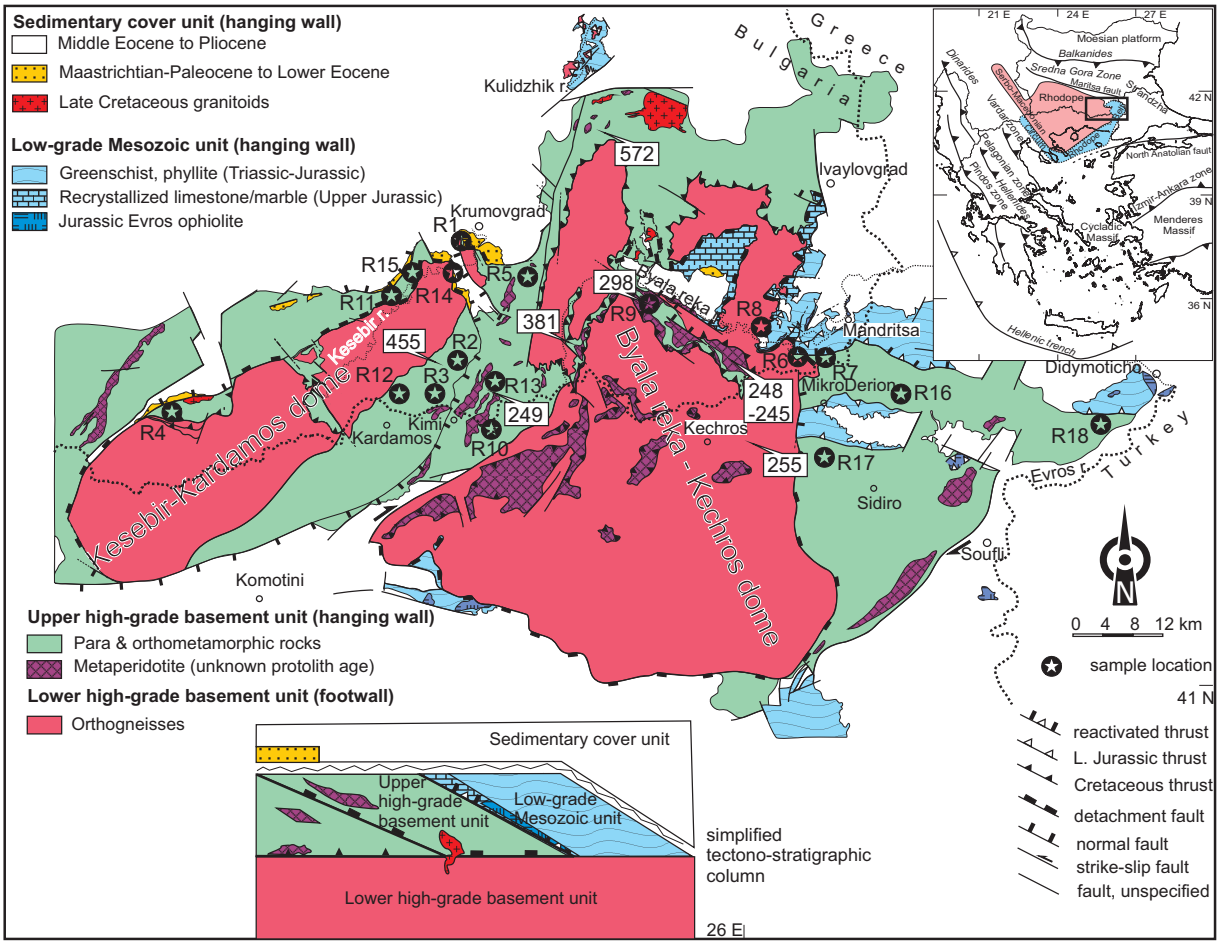

Fig. 1. Tectonic map of the eastern Rhodope Massif in southern Bulgaria and northern Greece, showing the locations of studied samples. Inset: The tectonic framework of the Alpine system in the northern Aegean region of the eastern Mediterranean (simplified after Bonev et al. 2015). For U–Pb zircon geochronology in boxes see text. The lower high-grade basement unit is the terminological equivalent of the lower allochthon (e.g. Janák et al. 2011, for a reference; Miladinova et al. 2018).

Geological outline

General

To the southwest, the southernmost parts of the Rhodope Massif are hidden in the Aegean Sea, and to the north, the Rhodope Massif is separated by the Maritza dextral strike-slip fault zone from the Late Cretaceous volcanic arc of the Sredna Gora Zone (Fig. 1, inset), underlying the sedimentary deposits of the large Cenozoic Thrace basin to the east (Fig. 1). The Rhodope Massif is regarded as a stack of syn-metamorphic nappes assembled by southward thrusting in the hanging wall of a north-dipping Late Cretaceous–Cenozoic subduction zone located in the Vardar Zone (Burg et al. 1996; Ricou et al. 1998; Burg 2012). Crustal thickening in the convergent region resulted in nappe stacking associated with the amphibolite-facies metamorphism that was accompanied by a coeval and subsequent extension (Koukouvelas & Doutsos 1990; Dinter & Royden 1993; Burg et al. 1996; Dinter 1998; Bonev et al. 2006; Bonev & Beccaletto 2007). The Rhodope Massif is dominated by amphibolite-facies metamorphic basement comprising pre-Alpine and Alpine (e.g. Lips et al. 2000; Liati 2005; Liati et al. 2011) units of continental and oceanic affinities that are intruded by voluminous Late Cretaceous to Miocene granitoids (Meyer 1968; Soldatos & Christofides 1986; Zagorchev et al. 1987; Dinter et al. 1995; Christofides et al. 2001; von Quadt & Peytcheva 2005; Marchev et al. 2013). Paleocene–Eocene to Pliocene–Quaternary sedimentary rocks (with internal unconformities) (Ivanov & Kopp 1969; Zagorchev 1998; Boyanov & Goranov 2001 and references therein) and Oligocene volcanic and volcanic-sedimentary successions (Innocenti et al. 1984; Del Moro et al. 1988; Harkovska et al. 1989; Christofides et al. 2004; Marchev et al. 2010) represent cover sequences.

Geological outline of the eastern Rhodope Massif

The regional tectonic pattern of the eastern Rhodope Massif is dominated by late Alpine extensional core complex-type metamorphic domes, namely the Kesebir–Kardamos and

the Byala reka–Kechros domes, exposing four main units in the tectono-stratigraphic pile (Fig. 1, Bonev 2006; Bonev et al. 2006). These units are predominantly bounded by extensional tectonic contacts of presently inactive Early Eocene low-angle detachments. They are subdivided according to their structural position, tectono-metamorphic history, and the radiometric ages of coherent lithologies in their footwalls and hanging walls. Structurally, from the base to the top, they are: (i) a lower high-grade unit, (ii) an upper high-grade unit, both constituting the high-grade metamorphic basement, (iii) an overlying low-grade Mesozoic unit, and (iv) a Maastrichtian–Paleocene to Pliocene sedimentary and volcanic unit of cover sequences, including voluminous Late Eocene–Oligocene volcanics and volcano-sedimentary successions (Fig. 1). In addition, the high-grade basement units are intruded by Late Cretaceous–Oligocene granitoids (Del Moro et al. 1988; Pe-Piper & Piper 2002; Ovtcharova et al. 2003; Marchev et al. 2006).

The lower high-grade basement unit in the footwall of the domes, having a clear continental origin, is mainly composed of orthogneisses and migmatites, with subordinate paragneiss and amphibolite intercalations. The orthogneisses have Late Carboniferous–Late Permian granitoid protolith ages in the range of 326–254 Ma as derived from U–Pb zircon geochronology (Peytcheva & von Quadt 1995; Cornelius 2008; Liati et al. 2011), indicating that Late Paleozoic (likely Variscan or Hercynian) crustal fragments were involved in the nappe stack during Alpine deformation.

The upper high-grade basement unit represents a lithologically heterogeneous succession of continental–oceanic affinity consisting of intercalated meta-sedimentary and meta-igneous rocks. This unit comprises widespread occurrences of ultramafic and mafic meta-ophiolite bodies. The protolith ages of the meta-igneous rocks (inclusive meta-ophiolite) in the upper high-grade basement unit span 572 Ma to 151 Ma age range (Carrigan et al. 2003; Cornelius 2008; Liati et al. 2011; Bonev et al. 2013a, 2015; Peytcheva et al. 2018) (see also Discussion section).

The dominant amphibolite-facies and relict eclogite-facies metamorphism in the eastern Rhodope high-grade basement units (Liati & Mposkos 1990; Mposkos & Liati 1993; Miladinova et al. 2018) locally reached ultra-high-pressure pressure conditions (Mposkos & Kostopoulos 2001), thus indicating that the rocks have suffered a complex Alpine tectono-metamorphic history, likely in different times from 158 Ma to 42 Ma (Liati 2005; Liati et al. 2011). However, both high-grade basement units in the eastern Rhodope region gradually cooled below 500–300 °C from the hanging wall to footwall of the extensional system in Paleocene to Late Eocene (63–34 Ma) times as derived from $^{40}Ar/^{39}Ar$ geochronology (e.g. Bonev et al. 2013b and references therein).

The Mesozoic (Triassic to Early Cretaceous) low-grade sequences (Papadopoulos et al. 1989; Boyanov et al. 1990) form a distinct unit, which is regarded as the eastern extension of the Circum-Rhodope Belt defined in the Chalkidiki Peninsula of northern Greece (e.g. Kauffmann et al. 1976; Papanikolaou 2009). This unit, forming part of the hanging wall, consists of Triassic–Late Jurassic in age of the protoliths metasandstone, marble, greenschist and phyllite (Meinhold & Kostopoulos 2013; Bonev et al. 2019a) and Early–Middle Jurassic island arc tholeiitic basalt-andesite lava flows, meta-pyroclastic rocks and intrusive rocks (Bonev et al. 2015 and references therein). Stratigraphically, they are overlain by Early Cretaceous limestone (Ivanova et al. 2015), which seals the Late Jurassic low-grade metamorphic and tectonic emplacement history (ca. 157–154 Ma, Bonev et al. 2010; Bonev & Stampfli 2011). Based on the petrology and geochemistry of the arc magmatic suite and the bulk lithologic context, the Mesozoic low-grade unit is interpreted as a Jurassic–Early Cretaceous island arc-accretionary assemblage, originally located along the northern active margin of the Vardar Ocean (Bonev & Stampfli 2003, 2008; Bonev et al. 2015).

The sedimentary and volcanic unit of cover sequences range in ages from the Maastrichtian–Paleocene to the Pliocene (Boyanov & Goranov 2001). The Maastrichtian–Paleocene to Middle Eocene sedimentary rocks form part of a syn-tectonic hanging wall suite of supra-detachment half-grabens, in fault contact with the detachment (Bonev et al. 2006), and are limited by graben-bounding faults or lying unconformably over the high-grade basement units. These sedimentary rocks are unconformably overlain by Upper Eocene–Oligocene sedimentary rocks, which mark the subsequent cycle of continental sedimentation. They were accompanied by Late Eocene–Oligocene volcanic and sedimentary-volcanogenic successions (Harkovska et al. 1989). The Miocene–Pliocene top sedimentary rocks represent a new transgressive cycle covering unconformably the metamorphic basement and the Paleogene successions.

Previous data on the mafic-ultramafic meta-ophiolitic rocks of the eastern Rhodope Massif

In the upper unit of the high-grade metamorphic basement ultramafic rocks are represented by numerous bodies and lenses consisting of restite peridotite (harzburgite) and cumulate peridotite (dunite–wehrlite–ortho- and clinopyroxenite) with MORB to supra-subduction zone (SSZ)-like signature (Bazylev et al. 1999; Kolcheva et al. 2000), which together with the low-K mafic volcanic and plutonic rocks are regarded as metamorphosed fragments of an ophiolite association (Kozhoukharova 1984a). According to Kozhoukharova (1984a) high-Ti, high-Al and high-Fe subgroups can be chemically distinguished within the meta-ophiolite association. Among the meta-mafic rocks, the most abundant rock types are meta-gabbro–norite, meta-gabbro, meta-gabbro–diorite, all turned into amphibolite, but preserving relics of primary magmatic minerals and texture (Kozhoukharova 1984a). These amphibolites resulted from the main amphibolite-facies metamorphism, but preserve relic high-pressure (eclogite) assemblages (i.e. eclogite–amphibolite, Mposkos & Perdikatsis 1989; Baziotis et al. 2008, 2014), and display MORB-like geochemistry of oceanic crust tholeiite basalt protolith

(Kolcheva & Eskenazy 1988). A geochemical study of the amphibolites in Greece has shown their magmatic origin, whose protoliths were tholeiites with oceanic floor MORB/IAT affinities, the latter affinity more pronounced in the amphibolites from the eastern Rhodope Massif (Mposkos et al. 1989). Haydoutov et al. (2004) have documented island-arc origin of the amphibolites, with an arc tholeiitic to boninitic affinity.

Magmatic U–Pb zircon crystallization ages of the protoliths of the amphibolites in the upper high-grade basement unit vary significantly. Carrigan et al. (2003) have reported an age of 572±5 Ma for a meta-gabbro, which now turned to be Middle Jurassic in age (166.8±0.96 Ma, Filipov et al. 2022). Ages of 380.9±1.9 Ma (Peytcheva et al. 2018) and 298.1 ±6.2 Ma (Bonev et al. 2019b) were reported in amphibolitized eclogites. Bauer et al. (2007) have reported a range of ages from 287±5.5 to 199±1.8 Ma in the cores of zircons from an eclogite. Liati et al. (2011) have reported ages of 255.8 ±2.1 Ma and ~250 Ma for gabbroic protolith of other eclogites. Several zircons in amphibolite yielded magmatic core ages at 850 Ma, 573 Ma, 502 Ma, 389 Ma and 249 Ma (Bonev 2015). MORB-IAT affinity meta-gabbro and meta-plagiogranite and garnet-amphibolite, which are interpreted to have protoliths formed in a back-arc rift-spreading setting, yielded a mean age of 455 Ma for the magmatic crystallization (Bonev et al. 2013a).

Field data

Within the upper high-grade basement unit, the amphibolites occur either as layers of varying thickness (up to several hundred meters) alternating with other metamorphic rock types, or as distinct lenses or boudins. Most commonly the layers are dominated by massive and banded amphibolite, defining together with the intercalated metasedimentary lithologies the metamorphic layering. This layering is delineated by alternating amphibole and plagioclase-rich bands (Fig. 2a, b). The amphibolite layers may well represent initially lava flows or dykes. The other commonly occurred textural type is garnet-amphibolite, which also demonstrates a well-developed foliation deflected around the garnet porphyroblasts (Fig. 2c). The two main textural types of amphibolite recognised often surround the individual peridotite bodies and lenses within the metamorphic section of the upper high-grade basement unit (Fig. 2d). Another field occurrence of the amphibolite is taking part of a distinct mafic-ultramafic thrust sheet, which is best exposed in the core of the Byala reka–Kechros dome either stitched between the lower unit orthogneisses or exposed as thrust erosional remnants (klippen) on top of the latter unit (see Fig. 1). Mafic thrust sheet also occurs within the core of the Kesebir–Kardamos dome. Field observations indicate that primary magmatic textural features of the amphibolite precursors are strongly obliterated by the experienced high-grade metamorphism, which has transposed the lithologic contacts mostly parallel or oblique to the main amphibolite-facies regional foliation.

Samples and analytical methods

Representative samples were collected from the amphibolites in the upper unit of the high-grade metamorphic basement. Eleven rock samples were collected from massive and banded amphibolite in both metamorphic domes, to which are added six samples from garnet-amphibolite (samples R1, R5, R9, R12, R14, R17) and a single sample comes from a peridotite (sample R10) (see Fig. 1 for sample location, Supplementary Table S1).

Electron microprobe mineral analyses were obtained by JEOL 8200 Superprobe instrument at the University of Lausanne (Switzerland). Operating conditions were 10 nA beam current at 15 kV accelerating voltage in 5μm spot-size analysis with 30 s for peak and background counting, using natural standards and PAP correction. Selected chemical compositions and structural formula of the mineral phases in the studied amphibolites are listed in Supplementary Table S2 and depicted in Fig. 3.

Whole-rock chemical analyses were performed by analytical facilities at the University of Lausanne (Switzerland) and calibrated against both international and internal standards. Major- and trace element concentrations were determined by X-ray fluorescence (XRF) on fused discs and pressed pellets, respectively, using a Philips PW 2400 spectrometer. Standards used were MFTH, AGV, QLO, GA, BHVO-1. Accuracy for the major elements is <1 % and for the trace elements <2 %. REE concentrations were analysed by laser inductively coupled plasma mass spectrometry (LA-ICP-MS) on a Perkin-Elmer 6100 ELAN instrument on fused discs, using NBS612 standards. The results of chemical analyses are listed in Supplementary Table S3. The low loss on ignition (LOI) values in the samples (with only a few exceptions with >2 wt. %) used as a measure of hydrothermal alteration attest for the minimal degree of alteration of the studied rocks.

Petrography and mineral chemistry

The petrographic features of the two main textural types of amphibolites are summarized in Supplementary Table S1 for the studied samples, including also the peridotite sample. The massive amphibolites are fine- to medium-grained homogeneous meso-melanocratic rocks with granoblastic texture. When banded, the amphibolites display compositional layering of alternating amphibole and plagioclase-rich domains of various thicknesses, which delineate a foliated texture from outcrop to thin section scale (Figs. 2a, 4b, c). Both, the massive and banded amphibolite mainly consists of amphibole and plagioclase, to which quartz, epidote ±Fe–Ti oxides, and occasionally biotite and muscovite complements the mineral assemblage as the minor mineral phases (Fig. 4a–c). Accessory minerals are titanite, zircon and apatite. Epidote-group minerals are products related to the metamorphic processes and mostly developed around the amphibole crystals that locally are also partly chloritized. Elongated amphiboles, as seen both

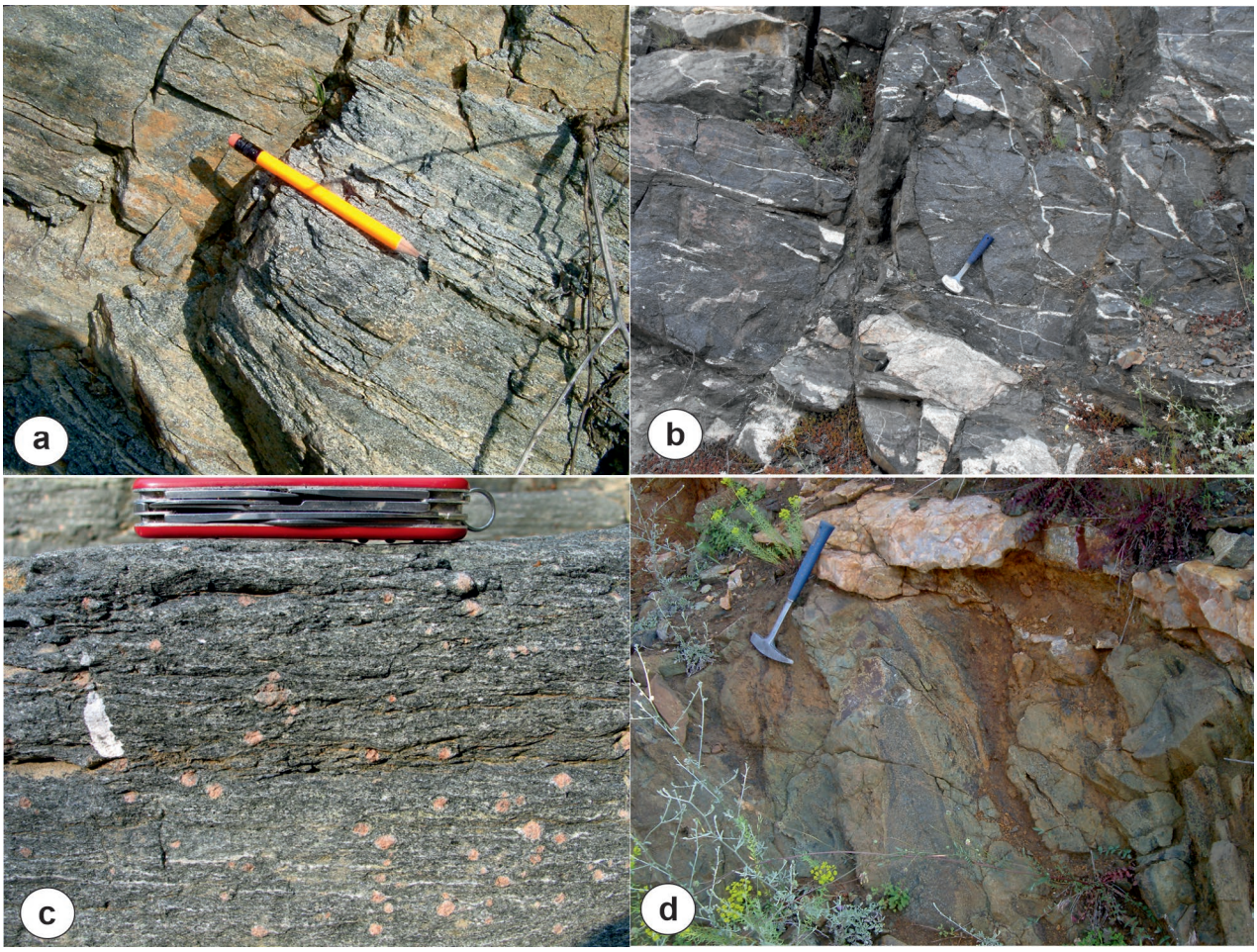

Fig. 2. Field photographs of the main textural types meta-mafic rocks. **a** — banded amphibolite; **b** — massive amphibolite; **c** — garnet-amphibolite; **d** — ultramafic rock lens.

in the field and in thin sections define the foliation (Fig. 4c). Amphiboles are magnesian-hastingsite hornblende and magnesian hastingsite (Fig. 3). The lamellar plagioclase, which generally preserved the original igneous grain shape and size (Fig. 4a, b), is unevenly altered to saussurite and epidote-group minerals (Supplementary Table S2).

The garnet-amphibolite displays granoblastic and mostly porphyroblastic texture, with high-grade metamorphic assemblage consisting of amphibole, plagioclase and garnet as the main constituent mineral phases, and a subordinate amount of epidote ±Fe–Ti oxides, titanite. Rutile, zircon and apatite are accessory mineral phases (Fig. 4d, e). Amphiboles have a range of the compositions from magnesio-hornblende, magnesio-hastingsite hornblende to edenite (Fig. 3). The plagioclase is oligoclase ($Ab_{89.04–74.94}$), and the unzoned garnet porphyroblasts have compositions mostly of almandine garnet, and occasionally possessing grossular-rich core ($Alm_{84.9–52.5}$ $Prp_{21.9–1.8}$ $Grs_{89.5–13.0}$) (Supplementary Table S2). Epidote-group minerals are related to the metamorphic processes, and developed both around the amphibole and plagioclase crystals.

Using the Al contents in the amphiboles, the metamorphic pressures can be estimated for amphibole crystallization (e.g. Anderson & Smith 1995). For the amphibolites pressures between 3–9 kbar were obtained on the basis of estimated lower limit of metamorphic temperatures of 570 °C by Miladinova et al. (2018) for the eclogite-facies metamorphism, which can be taken as an upper temperature limit of the amphibolite-facies metamorphism. These amphibolite-facies P–T estimates are consistent with P=6–2 kbar and T=630–520 °C obtained for amphibolites by Haydoutov et al. (2004). The majority of Al occurs as Al^{iv} reflecting relatively high-temperatures of crystallization (Supplementary Table S2), more likely close to T=630 °C.

The peridotite sample demonstrates fine- to medium-grained mesh texture dominated by olivine altered to serpentine-group minerals, together with subordinate mineral phases such as Fe–Ti oxide, chromite and spinel, all of them characteristic for dunite (Fig. 4f). It is not metamorphosed to a high-grade, and the observed dunite alteration is likely due to the initial ocean-floor low-grade hydrothermal metamorphism.

Overall, the textures, mineral assemblages and mineral compositions of the eastern Rhodope meta-mafic rocks turned into amphibolite point to high-grade metamorphic overprint in amphibolite-facies. The primary textures of the meta-mafic

rocks are largely obliterated by the high-grade metamorphism, and the rocks preserved partly the grain-sizes of the original igneous minerals. The meta-mafic rocks experienced lower amphibolite-facies to greenschist-facies metamorphism, the latter indicated by the chloritization of amphibole and calcite crystallization. Thus, the texture and mineral compositions are consistent with mafic igneous protoliths that underwent an amphibolite-facies degree of metamorphism, also indicated by the chemical composition (see below) of the meta-mafic rocks. Therefore, hereafter, we will use the term meta-mafic rocks.

Geochemistry

Because of the high-grade metamorphism experienced by the studied rocks, some mobility of the major and trace elements is expected despite their low LOI (Supplementary Table S3), and this may have provoked changes in the whole-rock chemical composition. The variation binary diagrams using highly immobile Zr and MgO as an index of differentiation have been used to evaluate the element mobility and to define geochemical trends (Figs. 5, 6). Meta-mafic rocks define linear trends and show a good correlation with MgO and Zr relative to major oxides and trace elements, indicating immobile behaviour of the trace elements and some minor elements. High- and low-Ti geochemical groups can be clearly distinguished on the basis of minor and trace elements contents (Figs. 5, 6). We interpret the immobile behaviour of the major oxides and trace elements as reflecting magmatic abundances and defining igneous differentiation trends. The exceptions are Na_2O, Rb and Sr that show scatter on the diagrams suggesting their mobility. This simple geochemical test allows the application of incompatible trace elements (e.g. Nb, Zr, Y) and rare earth elements (REE), which do not behave mobile during alteration and metamorphism, to be used effectively to demonstrate the chemical composition of the meta-mafic rocks. Therefore, the subsequent treatment of chemical data for evaluating geochemical signature, as well as tectonic setting discrimination of the meta-mafic rocks is based mainly on the immobile trace elements and REE.

The meta-mafic rocks cover the range mostly of basic to rarely intermediate compositions with SiO_2 (43–59 wt.%) (Supplementary Table S3). They are characterized by variable content of TiO_2 (0.26–3.76 wt.%), and consequently high-Ti (>1 wt.%) and low-Ti (<1 wt.%) groups can be distinguished on the basis of the Ti content (see also Fig. 5). The MgO content ranges from 4.2 to 10.69 wt.%. CaO content is moderate 5.84–14.61 wt.%, and Al_2O_3 ranges from 12.14 to 21.59 wt.%. Alkali contents are variable, generally elevated (av. total alkali >3 wt.%) with a high Na/K ratio (Supplementary Table S3). In a Zr/TiO_2 vs. Nb/Y diagram samples fall in the sub-alkaline basalt and andesite/basalt fields (Fig. 7a). The majority of samples plot in the tholeiitic field, and only one sample fall in the calc-alkaline field on the AFM diagram (Fig. 7b). In the latter diagram, iron enrichment is more pronounced for

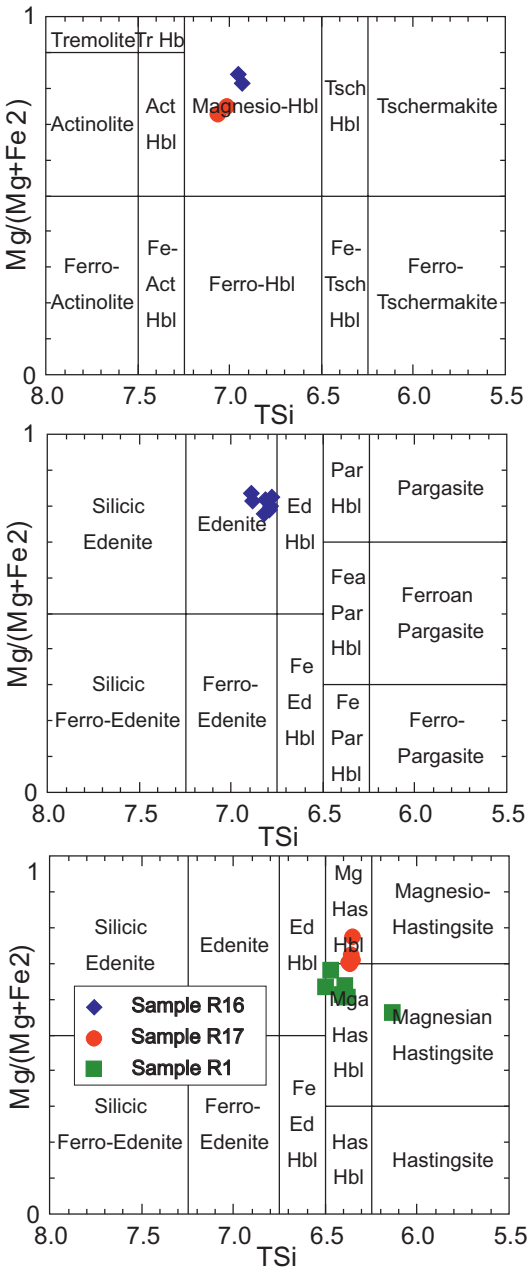

Fig. 3. Amphibole discrimination diagrams (nomenclature after Leake 1978) for the studied meta-mafic rocks.

the high-Ti group and thus consistent with the tholeiitic trend, which is also depicted in Fig. 7c.

In terms of the trace elements, the meta-mafic rocks show the following characteristics (Supplementary Table S3): (i) high abundances of incompatible elements (e.g. Nb, Y, Zr), (ii) variable, but overall similar Hf, Ta and Sc contents; (iii) relatively low Cr (27–483 ppm), with exception of a single sample, relatively elevated V (140–819 ppm) and low Ni (<200 ppm) concentrations. The low Ni and Cr contents in the meta-mafic rocks do not meet the criteria for primitive mantle-derived melts. Therefore, the major and trace element abundances of the meta-mafic rocks classify them as low-K

and low- to high-Ti tholeiitic affinity igneous protoliths of basaltic (gabbroic) to andesitic (dioritic) compositions. The dunite sample displays major and trace elements characteristics typical for a peridotite such as low SiO_2, and very high MgO, Cr and Ni concentrations (Supplementary Table S3).

The meta-mafic rocks display REE abundances higher than the chondrite, showing distinct patterns on chondrite-normalized diagrams (Fig. 8a, b). The high-Ti group meta-mafic rocks show flat REE profiles that characterize ocean floor basalts. Light rare earth element (LREE) abundances are intermediate between normal mid-ocean ridge basalt (N-MORB) plus enriched mid-ocean ridge basalt (E-MORB) and oceanic island basalt (OIB), and the heavy rare earth element (HREE) are overlapping or higher in their abundances

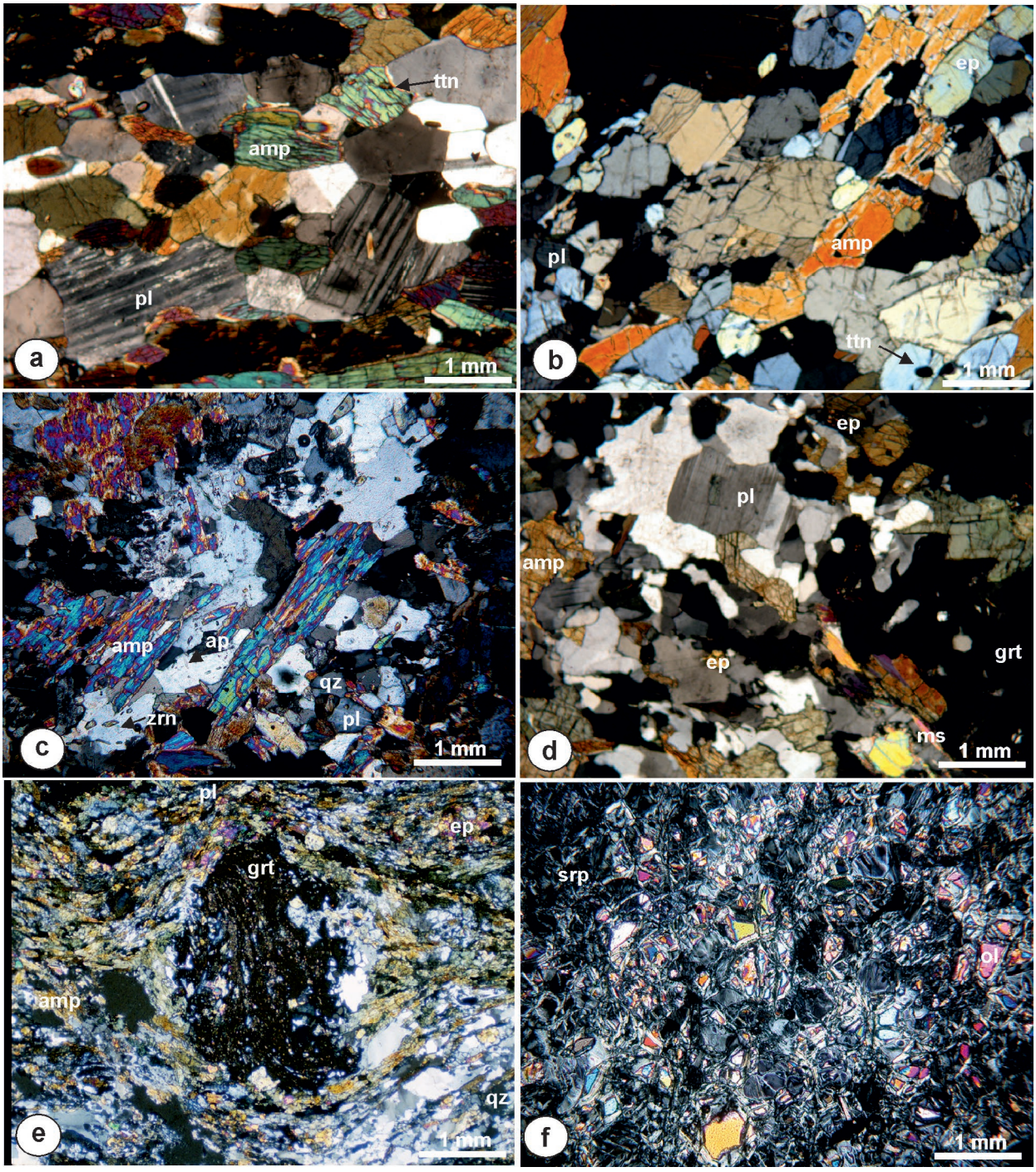

Fig. 4. Microphotographs of some of the studied meta-mafic rocks. **a** — sample R4; **b** — sample R16; **c** — sample R13; **d** — sample R3; **e** — sample R9; **f** — sample R10. Mineral abbreviations (after Whitney & Evans 2010): pl, plagioclase; amp, amphibole; grt, garnet; ap, apatite; ep, epidote; ttn, titanite; qz, quartz; zrn, zircon, ms, muscovite; srp, serpentine.

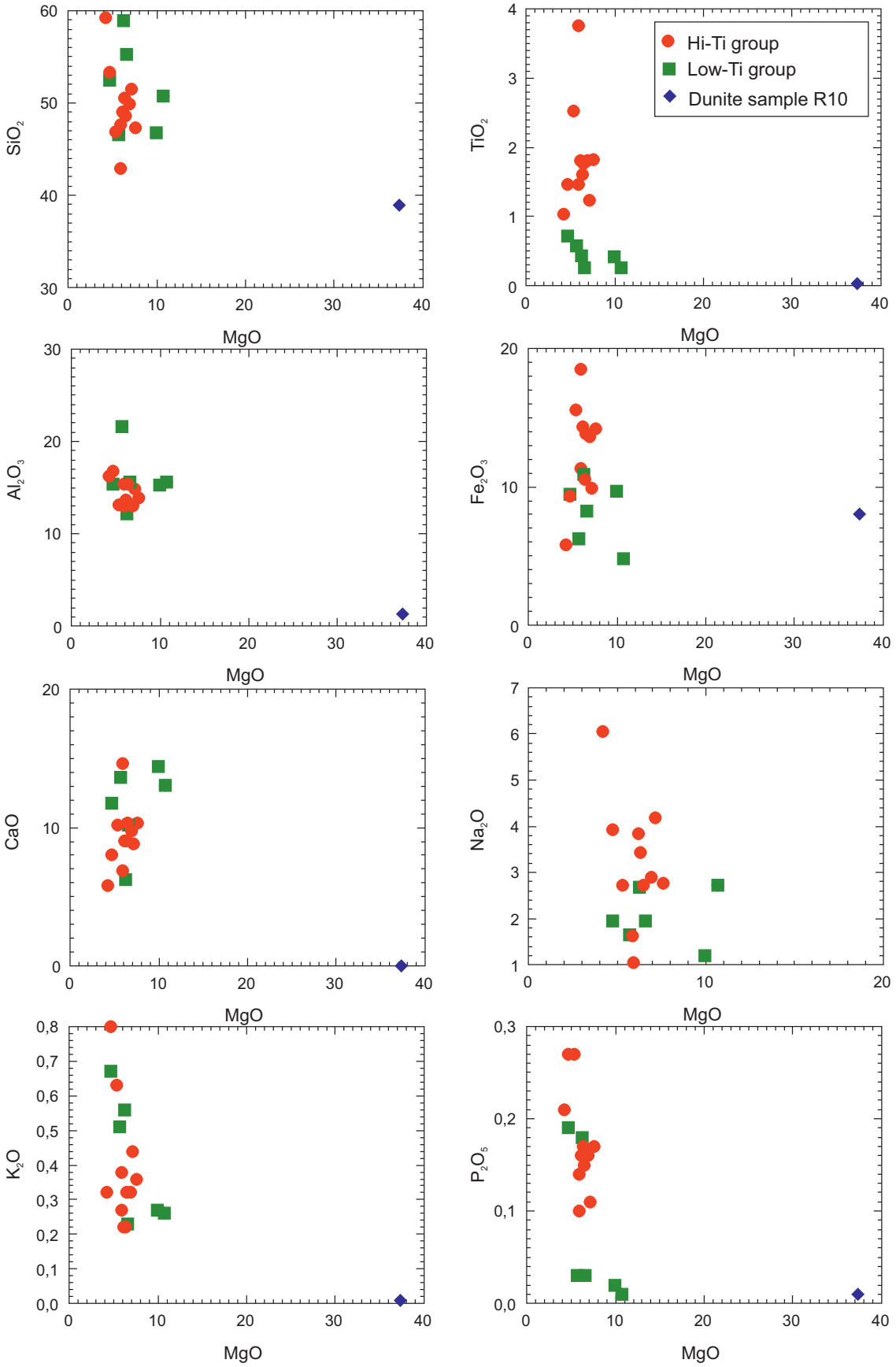

Fig. 5. Variation diagrams of selected major elements vs. MgO for the meta-mafic rocks (after Harker 1909).

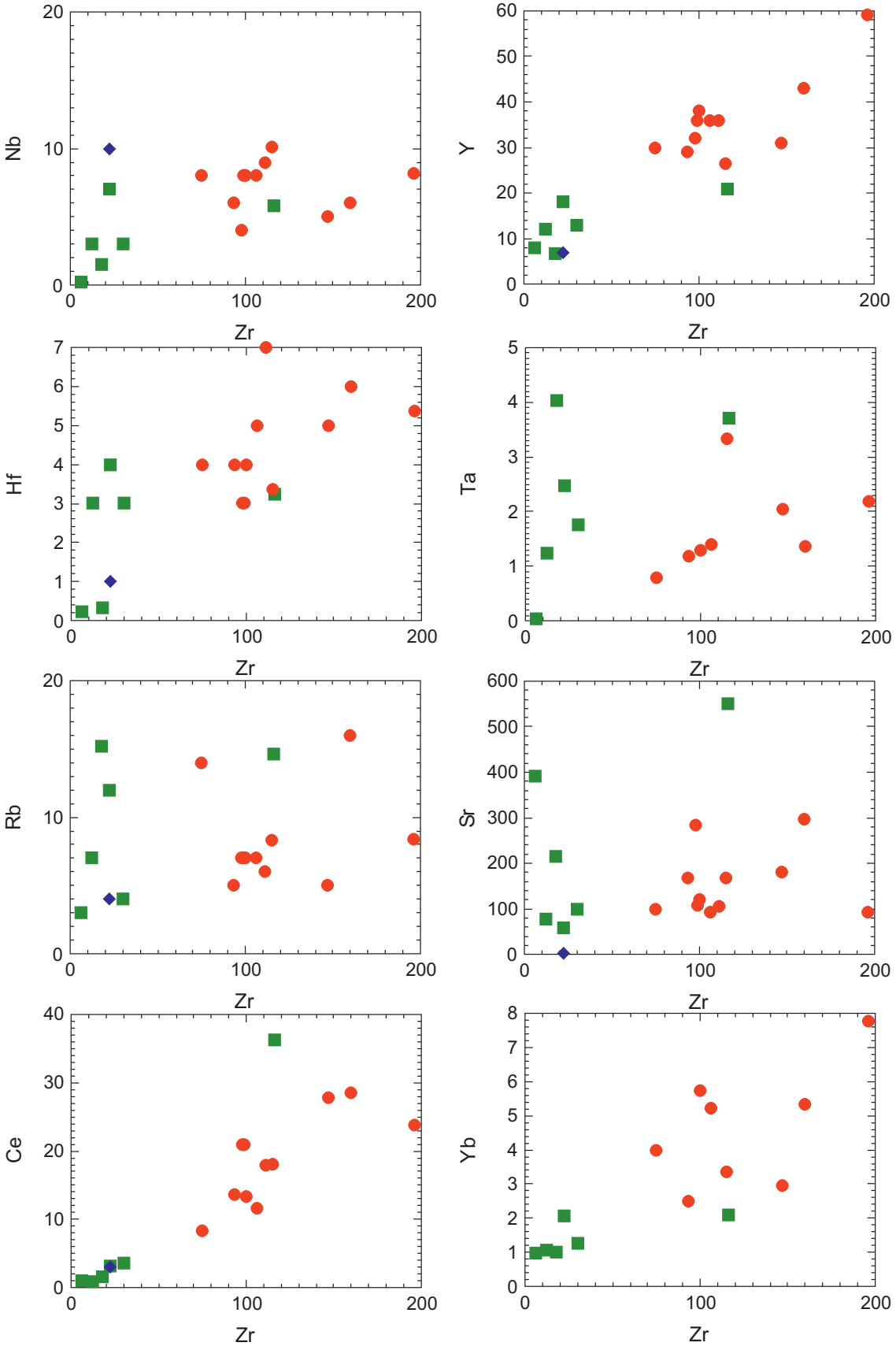

Fig. 6. Variation diagrams of selected trace elements vs. Zr for the meta-mafic rocks (after Harker 1909). Symbols same as in Fig. 5.

relative to these mantle sources (e.g. Sun & McDonough 1989, Fig. 8a). The REE profiles of low-Ti group meta-mafic rocks exhibit fractionation and deviate towards HREE-enriched patterns of various degree in absolute concentrations, but most of them are REE-depleted relative to N-MORB and E-MORB. Two samples demonstrate a weak U-shaped REE patterns that are characteristic for the boninite (e.g. Beccaluva & Serri 1988), and only a single sample shows OIB parallel REE profile (Fig. 8b). The weak positive or negative Eu anomalies suggest the involvement of the plagioclase in fractionation processes, particularly visible for the high-Ti group (Fig. 8a). Dunite sample displays LREE abundances close to and depleted relative to N-MORB in a way similar to the REE patterns of the low-Ti group meta-mafic rocks.

N-MORB normalized multi-element diagrams demonstrate high ratios of large-ion lithophile elements (LILE) and high-field strength elements (HFSE), considering that some LILE (e.g. Rb, K) were likely mobile (see Fig. 5). The high-Ti meta-mafic rocks show nearly flat HFSE and REE patterns close to N-MORB and mostly enriched than N-MORB in absolute abundances patterns from Lu to Sr, overlapping E-MORB and partly OIB compositions (Fig. 8c). The low-Ti meta-mafic rocks show more fractionated patterns with pronounced HFSE and REE depletion relative to N-MORB which is usually attributed to magmatic rocks related to island arc petrogenesis (Fig. 8d). The trace element patterns of the low-Ti group partly overlap those of the high-Ti group, displaying similarity of the patterns from Tb to Lu and the same bulk LILE enrichment. Nearly half of the low-Ti meta-mafic rocks are characterized by a negative Nb anomaly, while this anomaly in the other half of these rocks is always higher in Nb absolute abundances relative to N-MORB. A negative Nb anomaly in the high-Ti rocks is always higher in Nb absolute abundances relative to N-MORB. The high-Ti meta-mafic rocks display a slight positive Hf anomaly, which characterizes a half of the low-Ti rocks, and both groups show a negative P anomaly of various magnitudes. Both latter anomalies on N-MORB normalized diagrams imply the involvement of zircon and apatite in crystal fractionation processes. A negative Ti anomaly is also present in the group of low-Ti meta-mafic rocks. The dunite sample shows N-MORB normalized trace element profile similar to low-Ti meta-mafic rocks, as well as an analogous LREE-depleted (Ce and Nd) chondrite-normalized pattern.

The higher than N-MORB abundances of the HFSE and REE in the studied high-Ti meta-mafic rocks suggest an enriched magma source that deviates from the typical N-MORB, partly overlapping E-MORB LREE concentrations, but not so strongly LREE enriched compared to the OIB. Therefore, an E-MORB chemical signature with a likely mild OIB component in terms of middle rare earth element (MREE) and HREE is portrayed by the trace element and REE patterns of the high-Ti meta-mafic rocks. The profiles of HFSE and HREE-depleted low-Ti meta-mafic rocks typically deviate from N-MORB and E-MORB, while the LILE contents are comparable to the E-MORB and OIB abundances

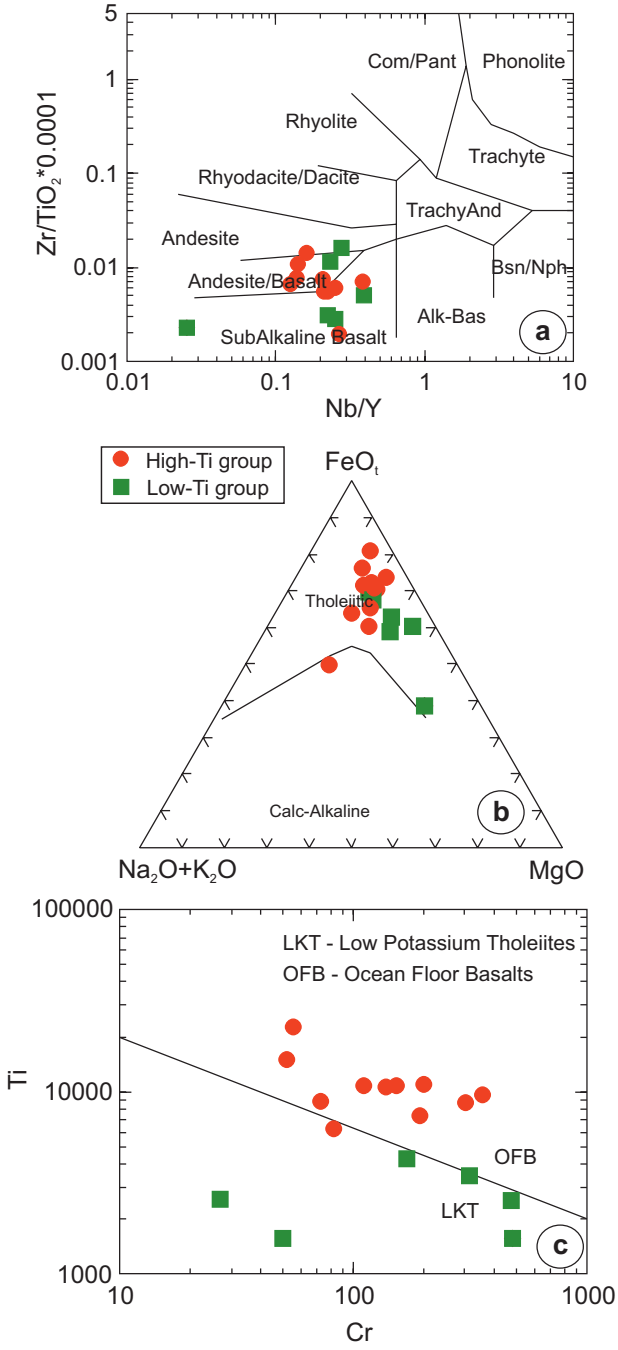

Fig. 7. Classification and geochemical affinity of the meta-mafic rocks. **a** — Zr/TiO_2 vs. Nb/Y plot (after Winchester & Floyd 1977); **b** — AFM diagram (after Irvin & Baragar 1971); **c** — Ti vs. Cr diagram (after Floyd & Winchester 1975).

(Fig. 8d). The low-Ti meta-mafic rocks, on the other hand, depict significantly depleted relative to N-MORB and partly to E-MORB chemical signatures, slightly comparable only to the signature of the LILE in the high-Ti group meta-mafic rocks.

The tectono-magmatic discrimination diagrams define an ocean floor affinity for the majority of the high-Ti group

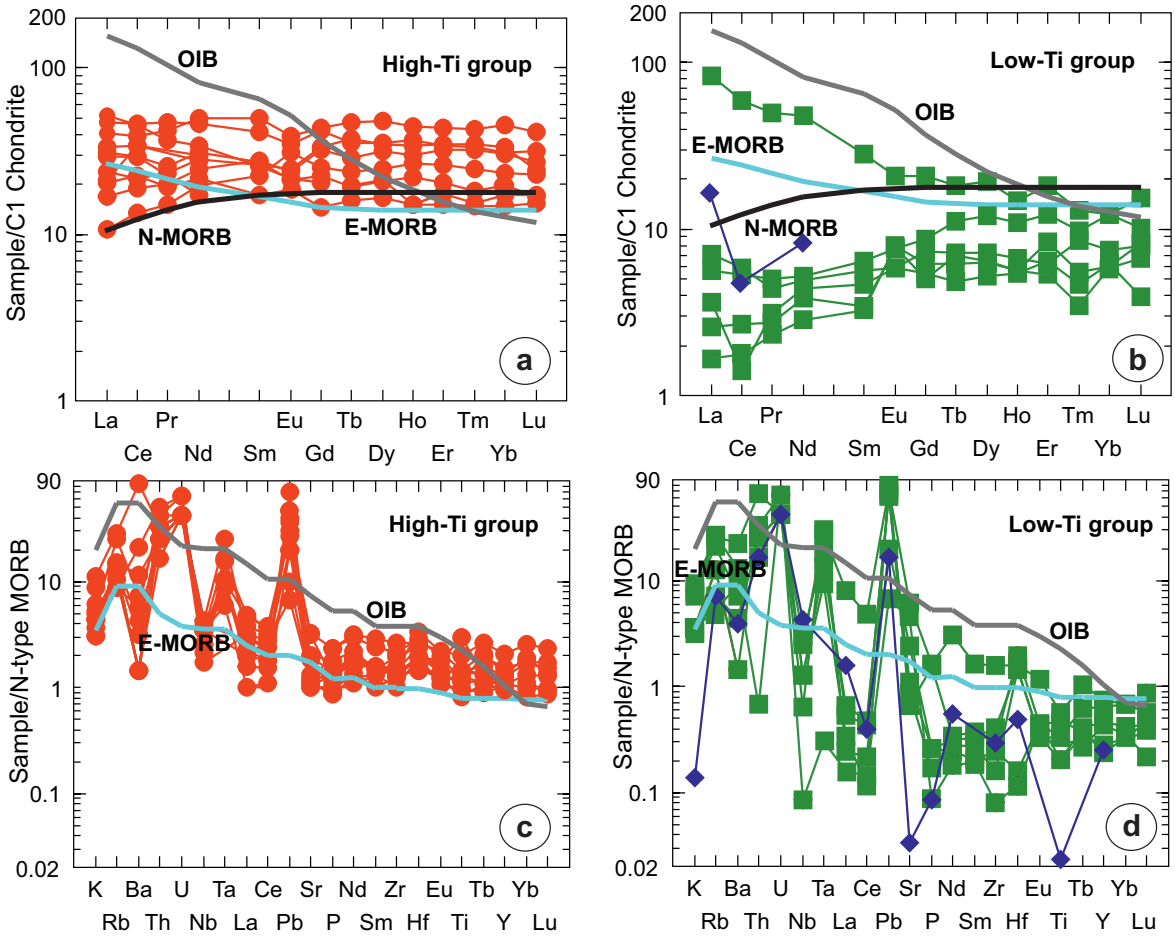

Fig. 8. a, b — Chondrite-normalized REE patterns, and **c, d** — N-MORB normalized diagrams for the meta-mafic rocks. Normalization values after Sun & McDonough (1989).

meta-mafic rocks in mid-ocean ridge (MORB) and within-plate (WPB) tectonic settings, and the rest have transitional MORB to island arc tholeiite (IAT) affinity (Fig. 9). The discrimination diagrams further display arc-related tectonic environment for the origin of the low-Ti meta-mafic rocks, which have also a mild MORB-like affinity. These inferred tectonic settings consistently reflect the geochemical signature and trace element and REE characteristics displayed by the studied meta-mafic rocks.

Discussion

Our petrographic results give evidence that in the upper high-grade basement unit of the eastern part of the Rhodope Massif the meta-mafic rocks have magmatic nature of their protoliths (basalt/gabbro to andesite/diorite, Fig. 7a). This is mostly revealed by preserved igneous grain shape and to a lesser extent size of the lamellar plagioclase in gabbroic varieties, which have experienced limited recrystallization during the metamorphic processes. Massive, and less frequently banded amphibolite, represents a good example for preserved igneous textures (Fig. 3a, b), whereas the metamorphic processes have strongly obliterated the magmatic textures of the garnet-amphibolite. Mineral compositions of amphibole and plagioclase in the meta-mafic rocks correspond to the dominant from an outcrop to thin section metamorphism in amphibolite-facies. These petrographic and mineralogical features are comparable to published analogous features (Kozhoukharova 1984b) and the P–T conditions for the amphibolite-facies metamorphism of the meta-mafic rocks (P=3–9 kbar at T=570 °C, this study) and associated rocks in the upper high-grade basement unit (e.g. Liati & Mposkos 1990; Mposkos & Liati 1993; Haydoutov et al. 2004; Mposkos et al. 2012). The petrographic results are further supported by the geochemical data obtained, but the geochemical types identified are irrespective relative to the textural types of the meta-mafic rocks i.e. amphibolites (Supplementary Table S3, see below).

Two geochemical types, namely the high-Ti and low-Ti groups of meta-mafic rocks, are distinguished based on Ti contents and trace element and REE characteristics of the analyzed meta-mafic rocks. The high-Ti rocks are indistinguishable from MORB-type tholeiites in terms of their HFSE and REE abundances and HREE normalized patterns. However, they overlap OIB, bearing also evidence for a weak

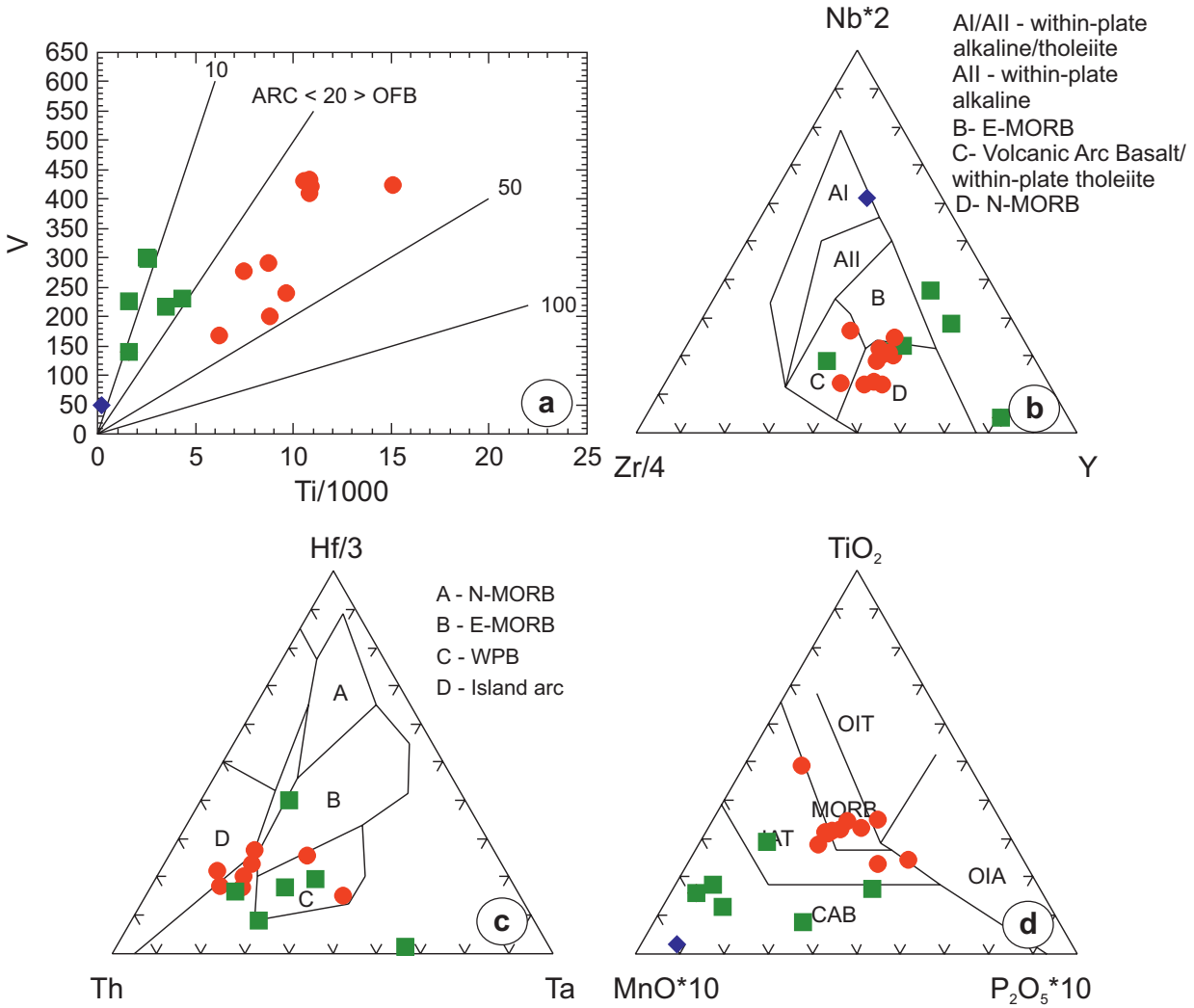

Fig. 9. Trace element tectonic setting discrimination diagrams for the meta-mafic rocks. **a** — Ti vs. V diagram (after Shervais 1982); **b** — Zr–Nb–Y diagram (after Meschede 1986); **c** — Th–Hf–Ta (after Wood 1980); **d** — MnO–TiO_2–P_2O_5 (after Mullen 1983).

geochemical fingerprint of subduction zone-related component in view of the high LILE/HFSE ratio (Fig. 8). However, HFSE-enriched patterns, particularly Ta and Nb contents higher than MORB abundances, as well as the fields where the high-Ti group rocks plot on the discrimination diagrams, suggest a contribution of the OIB component involved in the petrogenesis of magmatic precursors. Thus, the complex chemistry of high-Ti meta-mafic protoliths indicate their origin primarily from a depleted mantle source similar to MORB, substantially modified by subduction-zone derived LILE- and REE-enriched melts and contribution of HFSE-enriched component that produce the oceanic island tholeiites. The low-Ti group displays typical IAT affinity with a clearly defined subduction-related component, which is demonstrated by LILE enrichment, HFSE and HREE depletion relative to N-MORB and pronounced negative Nb anomaly and a weak negative Ti anomaly (Fig. 8), all indicative for magmatic rocks erupted in an island arc setting (e.g. Pearce 1982, 1984; McCulloch & Gamble 1991; Tatsumi & Eggins 1995).

The geochemical results arising from the investigation allow us to place some constraints on the petrogenesis of the meta-mafic rocks in the upper high-grade basement unit. In terms of the REE patterns, incompatible elements (e.g. Nb, Zr, Hf, Ti, Y, Yb) ascribed to a mantle component, high LILE/HFSE ratios that reflect subduction-related component (Pearce et al. 1984; Saunders & Tarney 1991), all are indicative of MORB mantle source, more depleted than that one which produces N-MORB for the low-Ti group, which is less depleted, enriched MORB for the high-Ti group. On a Th/Yb vs. Nb/Yb diagram samples plot in the volcanic arc array (Fig. 10a), with a high Th/Yb ratio, which is used as a proxy indicating crustal contamination or subduction component added as crustal input (Pearce & Peate 1995; Pearce 2008). In addition, on the TiO_2/Yb vs. Nb/Yb diagram a shallow melting in the crustal column is displayed by the majority of samples that fall in a MORB array, with low Ti/Yb ratios used as a proxy of melting depth (Pearce 2008). Thus, the Th/Yb–Nb/Yb–Ti/Yb ratios point to a detectable subduction zone influence related to mantle-crust

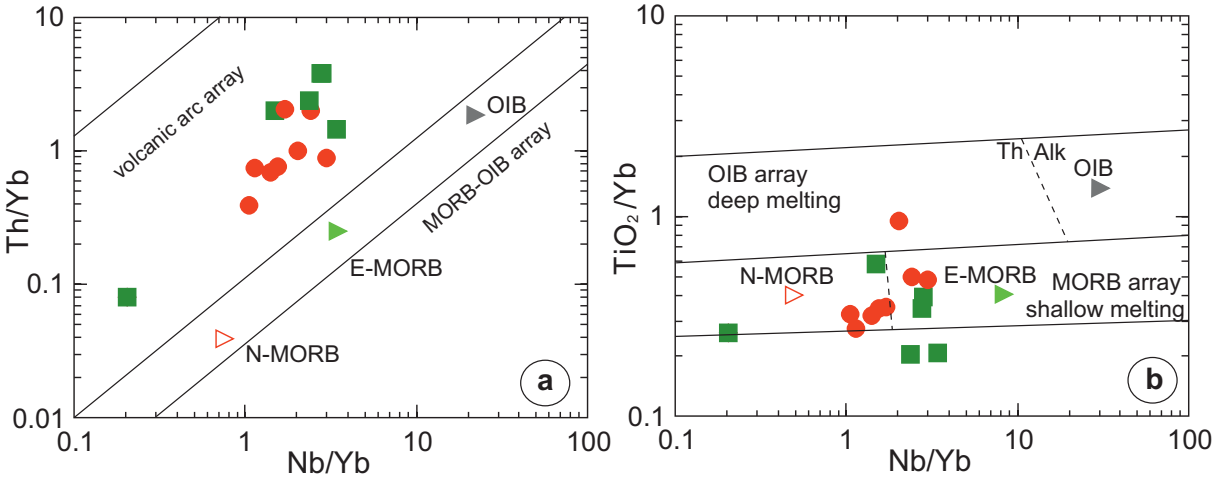

Fig. 10. a — Th/Yb vs. Nb/Yb diagram; **b** — TiO_2/Yb vs. Nb/Yb diagram (after Pearce 2008).

interaction in the melting column common for both geochemical groups, which have also partly overlapping aforementioned elemental ratios.

Compositional diversity of the meta-mafic rocks including magma types with MORB, transitional MORB/IAT and IAT affinity (Fig. 9), in turn, call for the origin of their protoliths in a paired ocean ridge-island arc environment. Modern analogues of such tectonic setting displaying transitional compositions between MORB and island-arc basalts are many back-arc basins (e.g. Saunders & Tarney 1984; 1991; Hawkins 1995; Fretzdorff et al. 2002; Taylor & Martinez 2003). Therefore, we attribute SSZ origin for the protoliths of meta-mafic rocks, which were generated in an island arc/back-arc setting (e.g. Pearce 2003). SSZ setting most completely characterizes the origin and geochemical affinity of the meta-mafic rocks, which is also consistent with previous data on the geochemistry of ophiolitic mafic–ultramafic assemblage. In this tectonic scenario, the low-Ti group arc tholeiitic to boninitic-like magmatic precursors trace subduction initiation or immature arc (e.g. Haydoutov et al. 2004, and this study), whereas MORB and transitional MORB/IAT-type of the high-Ti meta-mafic rocks recognized in the present study testify for the magmatic products erupted during subsequent evolution of the subduction zone that relates to rifting/sea-floor spreading, most likely in a back-arc setting. The incorporation of the fertile, less depleted mantle in a back-arc region can explain the HFSE and REE-enriched geochemical fingerprint observed in the high-Ti-group, which can be attributed to a variable degree of the partial melting of a MORB-type, and/or possibly mixing with enriched OIB-type source. The highly HFSE and REE-depleted low-Ti group point to residual, depleted MORB-type mantle source (Fig. 10), for which group melt generation is attributed to a distinct depleted source in a mantle wedge of the subduction system, substantially modified by the subduction process. The presence of Nb and Ti negative anomalies in low-Ti group rocks relative to MORB demonstrates the features characteristic for subduction-related magmas. The high LILE/HFSE ratios and positive Th, Pb Ta anomalies, which are common for both geochemical groups, in turn, testify for a chemically coupled arc/back-arc system. The lavas erupted in back-arc regions may plot in MORB, as well as in the IAT fields, showing an indication of island arc/back-arc origin (Beccaluva et al. 1983; Saunders & Tarney 1984; Dilek et al. 2007, 2008), and consequently, the meta-mafic rocks display both MORB and volcanic arc (IAT) signatures.

Carbonate and clastic turbidite-like metasedimentary successions of the upper high-grade basement unit associated with the meta-mafic ophiolitic rocks, which may represent deposits from distinct regions of the arc/back-arc system (e.g. fore-arc or intra-arc), fit the interpretation of an SSZ tectonic setting. However, the age of this arc/back-arc system is still poorly constrained despite a few available U-Pb zircon data for the meta-mafic rocks in the eastern Rhodope region (see Fig. 1). Published Middle–Late Ordovician (Bonev et al. 2013a), Late Devonian (Peytcheva et al. 2018), and Early Permian (Bonev et al. 2019b, for sample R9) ages, together with a single zircon aged at 249 Ma (Bonev 2015, in sample R13), as well as Early Triassic ages (247.8±2.3 Ma and 244.7 ±3.1 Ma, Bonev et al. 2022) for mafic dykes cross-cutting a dunite body (not that in this study, see Fig. 1), altogether indicate Middle-Late Paleozoic magmatic history of the meta-mafic rocks. As the Mid- to Late Paleozoic ages of the meta-mafic rocks predominate (same Late Paleozoic ages are also identified in the lower high-grade basement unit), which are clearly temporally decoupled from the Early Paleozoic ages, this suggest that the development of the inferred arc/back-arc system relates mostly to the ocean-floor magmatic evolution in the Paleotethyan realm.

Conclusions

- Textures, mineral assemblages and mineral compositions of the meta-mafic rocks point to metamorphic overprint in amphibolite-facies, which largely obliterated the primary

textures, and the meta-mafic rocks preserved partly the grain-sizes of the original igneous plagioclase. Overall, the petrographic features are consistent with mafic igneous protoliths that underwent amphibolite-facies metamorphism, which is also indicated by the chemical composition of the meta-mafic rocks.

- The major and trace elements classify the meta-mafic rocks as low-K and low- to high-Ti tholeiitic affinity igneous protoliths of basaltic (gabbroic) to andesitic (dioritic) compositions. High-Ti and low-Ti geochemical groups are identified on the basis of trace element and REE characteristics of the meta-mafic rocks. The high-Ti rocks are indistinguishable from MORB-type tholeiites in terms of their HFSE and REE abundances and HREE normalized patterns that overlap OIB, bearing evidence for a weak subduction signal indicated by the high LILE/HFSE ratio. HFSE-enriched patterns (Ta and Nb contents higher than MORB), as well as the fields where the high-Ti group rocks plot on the discrimination diagrams, suggest a contribution of the OIB component involved in their petrogenesis. A complex chemistry of high-Ti meta-mafic protoliths indicate their origin primarily from the MORB mantle source, subsequently modified by subduction-zone derived LILE- and REE-enriched melts and contribution of HFSE-enriched component that produce the oceanic island tholeiites. The low-Ti group displays typical IAT affinity with a clearly defined subduction-related component, which is demonstrated by LILE enrichment, HFSE and HREE depletion relative to N-MORB and negative Nb and Ti anomalies, all indicative for magmatic rocks erupted in an island arc setting. A single dunite sample studied also displays geochemical characteristics of the low-Ti group meta-mafic rocks.
- Geochemical diversity of meta-basic rocks with MORB, transitional MORB/IAT and IAT affinities hints their supra-subduction origin in an island arc/back-arc system, with identifiable arc-related and rifting/sea-floor spreading magmatic products represented by the low-Ti and high-Ti geochemical groups, respectively. The associated sedimentary package fits the interpretation of the SSZ origin, because the studied meta-mafic rocks in the upper high-grade basement unit of the eastern Rhodope Massif are intimately interstratified with metasedimentary successions of carbonate and clastic turbidite-like character.
- At present, the available Middle-Late Paleozoic/Early Triassic radiometric ages (from 381 Ma to 249 Ma) of the meta-mafic rocks predominate over the Early Paleozoic ages in these rocks (455 Ma), from which they are clearly temporally separated, and this suggest that the development of the inferred arc/back-arc system relates mostly to the ocean-floor magmatic evolution in the Paleotethyan realm.

Acknowledgements: This research was supported by the National Science Fund (Bulgaria) via contract KP-06-N54/5. We thank Thorsten Nagel and an anonymous reviewer for careful reading and constructively commenting on our manuscript. The technical support for XRF, LA-ICP-MS and microprobe analyses at the University of Lausanne is greatly acknowledged. We thank Evelyn Boneva for language proofreading.

References

Anderson J.L. & Smith D.R. 1995: The effects of temperature and fO_2 on the Al-in-hornblende barometer. *American Mineralogist* 80, 549–559. https://doi.org/10.2138/am-1995-5-614

Bauer C., Rubatto D., Krenn K., Proyer A. & Hoinkes G. 2007: A zircon study from the Rhodope metamorphic complex, N-Greece: Time record of a multistage evolution. *Lithos* 99, 207–228. https://doi.org/10.1016/j.lithos.2007.05.003

Baziotis I., Mposkos E. & Perdikatsis V. 2008: Geochemistry of amphibolitized eclogites and cross-cutting tonalitic-trondhjemitic dykes in the Metamorphic Kimi Complex in East Rhodope (N.E. Greece): implications for partial melting at the base of a thickened crust. *International Journal of Earth Sciences* 97, 459–477. https://doi.org/10.1007/s00531-007-0175-1

Baziotis I., Mposkos E. & Asimow P.D. 2014: Continental rift and oceanic protoliths of mafic-ultamafic rocks from the Kechros Complex, NE Rhodope (Greece): implications from petrography, major and trace-element systematics and MELTS modeling partial melting at the base of a thickened crust. *International Journal of Earth Sciences* 103, 981–1003. https://doi.org/10.1007/s00531-014-1007-8

Bazylev B.A., Zakariadze G.S., Zeljazkova-Panayotova M.D., Kolcheva K., Oběrhansli R. & Solovieva N.V. 1999: Petrology of ultrabasites from the ophiolitic association in crystalline basement of the Rhodope Massif. *Petrology* 7, 191–212 (in Russian).

Beccaluva L., Girolamo P.D., Macciotta G. & Morra V. 1983: Magma affinities and fractionation trends in ophiolites. *Ofioliti* 8, 307–324.

Beccaluva L. & Serri G. 1988: Boninitic and low-Ti subduction-related lavas from intraoceanic arc-backarc systems and low-Ti ophiolites: a reappraisal of their petrogenesis and original tectonic setting. *Tectonophysics* 146, 291–315.

Bonev N. 2006: Cenozoic tectonic evolution of the eastern Rhodope Massif (Bulgaria): basement structure and kinematics of syn- to postcollisional extensional deformation. In: Dilek, Y. & Pavlides S. (Eds.): Post-Collisional Tectonics and Magmatism in the Mediterranean Region and Asia. *Geological Society of America Special Paper* 409, 211–235. https://doi.org/10.1130/2006.2409(12)

Bonev N. 2015: Protoliths and metamorphic events in the high-grade metamorphic basement of the Eastern Rhodope: constraints from U-Pb zircon geochronology. In: *Proceedings of Annual Conference of the Bulgarian Geological Society "Geosciences 2015"*, 57–58.

Bonev N. & Beccaletto L. 2007: From syn- to post-orogenic Tertiary extension in the north Aegean region: constraints on the kinematics in the eastern Rhodope-Thrace, Bulgaria-Greece and the Biga Peninsula, NW Turkey. In: Taymaz T., YilmazY. & Dilek Y. (Eds.): The Geodynamics of the Aegean and Anatolia. *Geological Society of London Special Publication* 291, 113–142. https://doi.org/10.1144/SP291.6

Bonev N.G. & Stampfli G.M. 2003: New structural and petrologic data on Mesozoic schists in the Rhodope (Bulgaria): geodynamic implications. *Comptes Rendus Geoscience* 335, 691–699. https://doi.org/10.1016/S1631-0713(03)00122-6

Bonev N. & Stampfli G. 2008: Petrology, geochemistry and geodynamic implications of Jurassic island arc magmatism as revealed by mafic volcanic rocks in the Mesozoic low-grade sequence, eastern Rhodope, Bulgaria. *Lithos* 100, 210–233. https://doi.org/10.1016/j.lithos.2007.06.019

Bonev N. & Stampfli G. 2011: Alpine tectonic evolution of a Jurassic subduction-accretionary complex: deformation, kinematics and $^{40}Ar/^{39}Ar$ age constraints on the Mesozoic low-grade schists of the Circum-Rhodope belt in the eastern Rhodope–Thrace region, Bulgaria–Greece. *Journal of Geodynamics* 52, 143–167. https://doi.org/10.1016/j.jog.2010.12.006

Bonev N., Burg J.-P. & Ivanov Z. 2006: Mesozoic-Tertiary structural evolution of an extensional gneiss dome – the Kesebir-Kardamos dome, eastern Rhodope (Bulgaria-Greece). *International Journal of Earth Sciences* 95, 318–340. https://doi.org/10.1007/s00531-005-0025-y

Bonev N., Spikings R., Mortiz R. & Marchev P. 2010: The effect of early Alpine thrusting in late-stage extensional tectonics: Evidence from the Kulidzhik nappe and the Pelevun extensional allochthon in the Rhodope Massif, Bulgaria. *Tectonophysics* 488, 256–281. https://doi.org/10.1016/j.tecto.2010.01.001

Bonev N., Ovtcharova-Schaltegger M., Moritz R., Marchev P. & Ulianov A. 2013a: Peri-Gondwanan Ordovician crustal fragments in the high-grade basement of the Eastern Rhodope Massif, Bulgaria: evidence from U–Pb LA-ICP-MS zircon geochronology and geochemistry. *Geodinamica Acta* 26, 207–229. https://doi.org/10.1080/09853111.2013.858942

Bonev N., Spikings R., Moritz R., Marchev P. & Collings D. 2013b: $^{40}Ar/^{39}Ar$ age constraints on the timing of Tertiary crustal extension and its temporal relation to ore-forming and magmatic processes in the eastern Rhodope Massif, Bulgaria. *Lithos* 180–181, 264–278. https://doi.org/10.1016/j.lithos.2013.05.014

Bonev N., Marchev P., Moritz R. & Collings D. 2015: Jurassic subduction zone tectonics of the Rhodope Massif in the Thrace region (NE Greece) as revealed by new U–Pb and $^{40}Ar/^{39}Ar$ geochronology of the Evros ophiolite and high-grade basement rocks. *Gondwana Research* 27, 760–775. https://doi.org/10.1016/j.gr.2014.08.008

Bonev N., Filipov P. & Raicheva R. 2019a: Detrital zircon record on the stratigraphy of meta-carbonate rocks in the Circum-Rhodope Belt: U–Pb LA-ICP-MS geochronology data from the Mandritsa unit, Bulgaria. *Bulletin of the Geological Society of Greece, Special Publication* 7, Extended Abstract, 35–36.

Bonev N., Filipov P. & Raicheva R. 2019b: Age of the metaophiolites in the Eastern Rhodope Massif: Prototethys vs. Paleotethys connection. *Goldschmid Conference*, abstract 325.

Bonev N., Filipov P. & Dotseva Z. 2022: U–Pb zircon age constraint on a metaophiolite peridotite body from the high-grade metamorphic basement of the eastern Rhodope Massif, Bulgaria. In: 22th Congress of the *CBGA* Abstract Book. *Geologica Balcanica*, 273.

Boyanov I. & Goranov A. 2001: Late Alpine (Paleogene) superimposed depressions in parts of southeastern Bulgaria. *Geologica Balcanica* 31, 3–36. https://doi.org/10.52321/GeolBalc.31.3-4.3

Boyanov I., Ruseva M., Toprakcieva V. & Dimitrova E. 1990: Lithostratigraphy of the Mesozoic rocks from the Eastern Rhodopes. *Geologica Balcanica* 20, 3–28 (in Russian).

Burg J.-P. 2012: Rhodope: From Mesozoic convergence to Cenozoic extension. Review of petro-structural data in the geochronological frame. In: Skourtsos E. & Lister G.S. (Eds.): Geology of Greece. *Journal of the Virtual Explorer* 42, paper 1. https://doi.org/10.3809/jvirtex.2011.00270

Burg J-P., Ricou L-E., Ivanov Z., Godfriaux I., Dimov D. & Klain L. 1996: Syn-metamorphic nappe complex in the Rhodope Massif. Structure and kinematics. *Terra Nova* 8, 6–15. https://doi.org/10.1111/j.1365-3121.1996.tb00720.x

Carrigan C.W., Mukasa S.B., Haydoutov I. & Kolcheva K. 2003: Ion microprobe U-Pb zircon ages of pre-Alpine rocks in the Balkan, Sredna Gora and Rhodope terranes of Bulgaria: constraints on Neoproterozoic and Variscan tectonic evolution. *Journal of the Czech Geological Society* 48, 32–33.

Çelik Ö.F. 2002: Geochemical, petrological and geochronological observations on the metamorphic rocks of the Tauride belt ophiolites (S.Turkey). *Ph.D. thesis, University of Geneva*, no. 3371. https://doi.org/10.13097/archive-ouverte/unige:97980

Christofides G., Koroneos A., Soldatos T., Eleftheriadis G. & Kilias A. 2001: Eocene magmatism (Sithonia and Elatia plutons) in the internal Hellenides and implications for Eocene-Miocene geological evolution of the Rhodope Massif (Northern Greece). *Acta Vulcanologica* 13, 73–89.

Christofides G., Peckay Z., Elefteriadis G., Soldatos T. & Koroneos A. 2004: The Tertiary Evros volcanic rocks (Thrace, northernmost Greece): petrology and K/Ar geochronology. *Geologica Carpathica* 55, 397–409.

Cornelius N.K. 2008: UHP metamorphic rocks from the Eastern Rhodope Massif, NE Greece: new constraints from petrology, geochemistry and zircon ages. *Ph.D. thesis, University of Mainz*, 1–173.

Daşçı H.T., Parlak O., Nurlu N. & Billor Z. 2015: Geochemical characteristics and age of metamorphic sole rocks within a Neotethyan ophiolitic mélange from Konya region (central southern Turkey). *Geodinamica Acta* 27, 223–243. https://doi.org/10.1080/09853111.2014.979532

Del Moro A., Innocenti F., Kyriakopoulos C., Manetti P. & Papadopoulos P. 1988: Tertiary granitoids from Thrace (northern Greece): Sr isotopic and petrochemical data. *Neues Jahrbuch für Geologie und Paläontologie Abhandlungen* 159, 113–135.

Dilek Y., Furnes H. & Shallo M. 2007: Suprasubduction zone ophiolite formation along the periphery of Mesozoic Gondwana. *Gondwana Research* 11, 453–475. https://doi.org/10.1016/j.gr.2007.01.005

Dilek Y., Furnes H. & Shallo M. 2008: Geochemistry of the Jurassic Mirdita ophiolite (Albania) and the MORB to SSZ evolution of a marginal basin oceanic crust. *Lithos* 100, 174–209. https://doi.org/10.1016/j.lithos.2007.06.026

Dinter D.A. 1998: Late Cenozoic extension of the Alpine collisional orogen, northeastern Greece: Origin of the north Aegean basin. *Geological Society of America Bulletin* 110, 1208–1230.

Dinter D.A. & Royden L. 1993: Late Cenozoic extension in northeastern Greece: Strymon valley detachment system and Rhodope metamorphic core complex. *Geology* 21, 45-48.

Dinter D.A., Macfarlane A.M., Hames W., Isachsen C., Bowring S. & Royden L. 1995: U–Pb and $^{40}Ar/^{39}Ar$ geochronology of the Symvolon granodiorite: implications for the thermal and structural evolution of the Rhodope metamorphic core complex, northeastern Greece. *Tectonics* 14, 886–908.

Filipov P., Ichev M., Bonev N., Georgiev S. & Dotseva Z. 2022: LA-ICP-MS U–Pb zircon age of amphibolite protoliths associated with metaophiolites near the villages of Dobromirtsi and Bubino, east Rhodopes, Bulgaria. In: 22th Congress of the *CBGA* Abstract Book. *Geologica Balcanica*, 275.

Floyd P.A. & Winchester J.A. 1975: Magma type and tectonic setting discrimination using immobile elements. *Earth and Planetary Science Letters* 27, 211–218.

Fretzdorff S., Livermore R.A., Devey C., Leat P.T. & Stoffers P. 2002: Petrogenesis of the back-arc East Scotia ridge, South Atlantic Ocean. *Journal of Petrology* 43, 1435–1467. https://doi.org/10.1093/petrology/43.8.1435

Gartzos E., Dietrich V.J., Migiros G., Serelis K. & Lymperopoulou T. 2009: The origin of amphibolites from metamorphic soles beneath the ultramafic ophiolites in Evia and Lesvos (Greece) and their geotectonic implication. *Lithos* 108, 224–242. https://doi.org/10.1016/j.lithos.2008.09.013

Harker A. 1909: The natural history of the igneous rocks. *The Journal of Geology* 17, 488–489.

Harkovska A., Yanev Y. & Marchev P. 1989: General features of the Paleogene orogenic magmatism in Bulgaria. *Geologica Balcanica* 19, 37–72.

Hawkins J.W. 1995: The geology of Lau Basin. In: Taylor B. (Ed.): Back-arc Basins: Tectonics and Magmatism. *Plenum Press,* New York, 63–138.

Haydoutov I., Kolcheva K., Daieva L.A, Savov I. & Carrigan C.W. 2004: Island arc origin of the variegated formations from the east Rhodope, Bulgaria - implications for the evolution of the Rhodope massif. *Ofioliti* 29, 145–157.

Höhn M., Bröcker M. & Berndt J. 2022: The Jurassic meta-ophiolitic rocks of Cape Steno, Andros, Greece: a high-pressure/low-temperature mélange with Pelagonian affinity in the Cycladic Blueschist unit? *International Journal of Earth Sciences* 111, 949–968. https://doi.org/10.1007/s00531-022-02161-w

Innocenti F., Kolios N., Manetti P., Mazzuoli R., Peccerillo A., Rita F. & Villari L. 1984: Evolution and geodynamic significance of Tertiary orogenic volcanism in northeastern Greece. *Bulletin of Vulcanology* 47, 25–37.

Ivanov R. & Kopp K.O.1969: Das Alttertiär Thrakiens und der Ostrhodope. *Geology and Paleontology* 3, 123–153.

Ivanova D., Bonev N. & Chatalov A. 2015: Biostratigraphy and tectonic significance of lowermost Cretaceous carbonate rocks of the Circum-Rhodope Belt (Chalkidiki Peninsula and Thrace region, NE Greece). *Cretaceous Research* 52, 25–63. https://doi.org/10.1016/j.cretres.2014.08.003

Irvin T.H. & Baragar W.R.A. 1971: A guide to the chemical classification of the common volcanic rocks. *Canadian Journal of Earth Sciences* 8, 523–548.

Janák M., Froitzheim N. Georgiev N. Nagel T.J. & Sarov S. 2011: P–T evolution of kyanite eclogite from the Pirin Mountains (SW Bulgaria): implications for the Rhodope UHP Metamorphic Complex. *Journal of Metamorphic Geology* 29, 317–332. https://doi.org/10.1111/j.1525-1314.2010.00920.x

Kauffmann G., Kockel F. & Mollat H. 1976: Notes on the stratigraphic and paleogeographic position of the Svoula formation in the Innermost Zone of the Hellenides (Northern Greece). *Bulletin de la Societe Géologique de France* 18, 225–230.

Kolcheva K. & Eskenazy G. 1988: Geochemistry of metaeclogites from the Central and Eastern Rhodope Mts (Bulgaria). *Geologica Balcanica* 18, 61–78.

Kolcheva K., Haydoutov I. & Daieva L. 2000: Dismembered ultramafic ophiolites from the Avren synform, Eastern Rhodopes. *Geochemistry, Mineralogy and Petrology (Sofia)* 37, 27–38.

Koukouvelas I. & Doutsos T. 1990: Tectonic stages along a traverse cross-cutting the Rhodopian zone (Greece). *Geologische Rundschau* 79, 753–776.

Kozhoukharov D., Kozhoukharova E. & Papanikolau D. 1988: Precambrian in the Rhodope massif. In: Zoubek V., Cogné J., Kozhoukharov D. & Kräutner H.G. (Eds.): Precambrian in Younger Fold Belts - European Variscides, the Carpathians and Balkans. *John Willey and Sons,* Chichester, 723–778.

Kozhoukharova E. 1984a: Origin and structural position of the serpentinized ultrabasic rocks of the Precambrian ophiolitic association in the Rhodope Massif. I. Geologic position and composition of ophiolite association. *Geologica Balcanica* 14, 9–36.

Kozhoukharova E. 1984b: Origin and structural position of the serpentinized ultrabasic rocks of the Precambrian ophiolitic association in the Rhodope Massif. II. Metamorphic alteration of ultrabasics. *Geologica Balcanica* 14, 3–35.

Leake B.E. 1978: Nomenclature of amphiboles. *Mineralogical Magazine* 42, 533–563.

Liati A. 2005: Identification of repeated Alpine (ultra) high-pressure metamorphic events by U–Pb SHRIMP geochronology and REE geochemistry of zircon: the Rhodope zone of Northern Greece. *Contributions to Mineralogy and Petrology* 150, 608–630. https://doi.org/10.1007/s00410-005-0038-3

Liati A. & Mposkos E. 1990: Evolution of eclogites in the Rhodope zone of northern Greece. *Lithos* 25, 89–99.

Liati A., Gebauer D. & Fanning C.M. 2011: Geochronology of the Alpine UHP Rhodope zone: A review of isotopic ages and constraints on the geodynamic evolution. In: Dobrzhinetskaya L.F., Faryad S.W., Wallis S. & Cuthbert S. (Eds.): Ultrahigh-Pressure Metamorphism 25 Years after the Discovery of Coesite and Diamond. *Elsevier,* Amsterdam, 295–324.

Lips A.L.W., White S.H. & Wijbrans J.R. 2000: Middle-Late Alpine thermotectonic evolution of the southern Rhodope Massif, Greece. *Geodinamica Acta* 13, 281–292.

Marchev P., von Quadt A., Peytcheva I. & Ovtcharova M. 2006: The age and origin of the Chuchuliga and Rozino granites, Eas tern Rhodopes. In: *Proceedings of the Annual Conference of the Bulgarian Geological Society "Geosciences 2006"*, 213–216.

Marchev P., Kibarov P., Spikings R., Ovtcharova M., Márton I. & Moritz R. 2010: $^{40}Ar/^{39}Ar$ and U–Pb geochronology of the Iran Tepe volcanic complex, Eastern Rhodopes. *Geologica Balcanica* 39, 3–12. https://doi.org/10.52321/GeolBalc.39.3.3

Marchev P., Georgiev S., Raicheva R., Peytcheva I., von Quadt A., Ovtcharova M. & Bonev N. 2013: Adakitic magmatism in post-collisional setting: An example from the Early-Middle Eocene magmatic belt in South Bulgaria and North Greece. *Lithos* 180–181, 159–180. https://doi.org/10.1016/j.lithos.2013.08.024

McCulloch M.T. & Gamble J.A. 1991: Geochemical and geodynamical constraints on subduction zone magmatism. *Earth and Planetary Science Letters* 102, 358–374.

Meinhold G. & Kostopoulos D. 2013: The Circum-Rhodope Belt, northern Greece: Age, provenance, and tectonic setting. *Tectonophysics* 595–596, 55–68. https://doi.org/10.1016/j.tecto.2012.03.034

Meschede M. 1986: A method of discriminating between different types of mid-ocean ridge basalts and continental tholeiites with the Nb–Zr–Y diagram. *Chemical Geology* 56, 207–218.

Meyer W. 1968: Alterstellung des Plutonismus im Sdteil der Rila–Rhodope–Masse. *Geology and Paleontology* 2, 177–192.

Miladinova I., Froitzheim N., Nagel T., Janák M., Georgiev N., Fonseca R.O.C., Sandmann S. & Munker C. 2018: Late Cretaceous eclogite in the Eastern Rhodopes (Bulgaria): evidence for subduction under the Sredna Gora magmatic arc. *International Journal of Earth Sciences* 107, 973–996. https://doi.org/10.1007/s00531-018-1589-7

Mposkos E.D. & Kostopoulos D.K. 2001: Diamond, former coesite and supersilicic garnet in metasedimentary rocks from the Greek Rhodope: a new ultrahigh-pressure metamorphic province established. *Earth and Planetary Science Letters* 192, 497–506. https://doi.org/10.1016/S0012-821X(01)00478-2

Mposkos E. & Liati A. 1993: Metamorphic evolution of metapelites in the high-pressure terrane of the Rhodope zone, northern Greece. *Canadian Mineralogist* 31, 401–424.

Mposkos E. & Perdikatsis B. 1989: Eclogite-amphibolites in the east Rhodope. *Geologica Rhodopica* 1, 160–168.

Mposkos E., Perdikatsis B. & Liati A. 1989: Geochemical investigation of amphibolites from eastern and central Rhodope. *Bulletin of the Geological Society of Greece* 23, 413–425.

Mposkos E., Baziotis I. & Proyer A. 2012: Pressure-temperature evolution of eclogites from the Kechros complex in the Eastern Rhodope (NE Greece). *International Journal of Earth Sciences* 101, 2083–2099. https://doi.org/10.1007/s00531-011-0699-2

Mullen E.D. 1983: $MnO/TiO_2/P_2O$: a minor element discrimination for basaltic rocks of oceanic environments and its implications for petrogenesis. *Earth and Planetary Science Letters* 62, 53–62.

Nurlu N. 2020: U–Pb zircon geochronology and geochemistry of the metamorphic sole rocks of the Meydan mélange, South-East Turkey: Implications for ophiolite emplacement and protolith. *Geologica Carpathica* 71, 183–205. https://doi.org/10.31577/GeolCarp.71.2.6

Ovtcharova M., von Quadt A., Heinrich C.A., Frank M., Kaiser-Rohmeier M., Peycheva I. & Cherneva Z. 2003: Triggering of hydrothermal ore mineralization in the Central Rhodopean Core Complex (Bulgaria)-insight from isotope and geochronological studies on tertiary magmatism and migmatisation. In: Eliopoulos et al. (Eds.): Mineral Exploration and Sustainable Development, 1. *Millpress,* Rotterdam, 367–370.

Papadopoulos P., Arvanitidis N. & Zanas I. 1989: Some preliminary geological aspects on the Makri unit (Phyllite series), Peri-Rhodope Zone. *Geologica Rhodopica* 1, 34–42.

Papanikolaou D. 2009: Timing of tectonic emplacement of the ophiolites and terrane paleogeography in the Hellenides. *Lithos* 108, 262–280. https://doi.org/10.1016/j.lithos.2008.08.003

Papanikolaou D. 2013: Tectonostratigraphic models of the Alpine terranes and subduction history of the Hellenides. *Tectonophysics* 595–596, 1–24. https://doi.org/10.1016/j.tecto.2012.08.008

Parlak O., Yilmaz H. & Boztuğ D. 2006: Origin and tectonic significance of the metamorphic sole and isolated dykes of the Divriği ophiolite (Sivas, Turkey): Evidence for slab break-off prior to ophiolite emplacement. *Turkish Journal of Earth Sciences* 15, 25–45.

Pearce J.A. 1982: Trace element characteristics of lavas from destructive plate boundaries. In: Thorpe R.S. (Ed.): Andesites: Orogenic Andesites and Related Rocks. *John Wiley and Sons,* Chichester, 525–548,

Pearce J.A. 2003. Supra-subduction zone ophiolites: The search for modern analogues. In: Dilek Y. & Newcomb S. (Eds.): Ophiolite concept and the evolution of geological thought. *Geological Society of America Special Paper* 373, 269–293. https://doi.org/10.1130/0-8137-2373-6.269

Pearce J.A. 2008: Geochemical fingerprinting of oceanic basalts with applications to ophiolite classification and the search for Archean oceanic crust. *Lithos* 100, 14–48. https://doi.org/10.1016/j.lithos.2007.06.016

Pearce J.A., Lippard S.J. & Roberts S. 1984: Characteristics and tectonic significance of supra-subduction zone ophiolites. In: Kokelaar B.P. & Howells M.F. (Eds.): Marginal Basin Geology: Volcanic and Associated Sedimentary and Tectonic Processes in Modern and Ancient Marginal Basins. *Geological Society of London Special Publication* 16, 77–94.

Pearce J.A. & Peate D.W 1995: Tectonic implications of the composition of volcanic arc magmas. *Annual Review of Earth Sciences* 23, 251–285.

Pe-Piper G. & Piper D.J.W. 2002 : The igneous rocks of Greece. The anatomy of an orogen. *Gebrueder Borntraeger*, Berlin-Stuttgart, 1–573.

Peytcheva I. & von Quadt A. 1995: U-Pb zircon dating of metagranites from Byala Reka region in the east Rhodopes, Bulgaria. In: Papanikolaou D. (Ed.): Proceedings of XV Congress of the CBGA. *Geological Society of Greece Special Publication* 4, 637–642.

Peytcheva I., von Quadt A., Macheva L., Kolcheva K. & Sarov S. 2018: Relics of Devonian oceanic lithosphere in Byala Reka dome, Eastern Rhodopes: Evidence from zircon U–Pb dating and Hf-isotope tracing. *Comptes Rendus de l'Academie bulgare des Sciences* 71, 1657–1664. https://doi.org/10.7546/CRABS.2018.12.10

Robertson A.H.F. 2002: Overview of the genesis and emplacement of Mesozoic ophiolites in the Eastern Mediterranean Tethyan region. *Lithos* 65, 1–67.

Robertson A.H.F., Dixon J.E., Brown S., Collins A., Morris A., Pickett E., Sharp I. & Ustaömer T. 1996: Alternative tectonic models for the Late Palaeozoic-Early Tertiary development of Tethys in the Eastern Mediterranean region. In: Morris A. & Tarling D.H. (Eds.): Paleomagnetism and Tectonics of the Mediterranean Region. *Geological Society of London Special Publication* 105, 239–263.

Ricou L.-E., Burg J.-P., Godfriaux I. & Ivanov Z. 1998: The Rhodope and Vardar: the metamorphic and the olistostromic paired belts related to the Cretaceous subduction under Europe. *Geodinamica Acta* 11, 285–309.

Saunders A.D. & Tarney J. 1984: Geochemical characteristics of basaltic volcanism within back-arc basins. In: Kokelaar B.P. & Howells M.F. (Eds.): Marginal Basin Geology: Volcanic and Associated Sedimentary and Tectonic Processes in Modern and Ancient Marginal Basins. *Geological Society of London Special Publication* 16, 59–76.

Saunders A. & Tarney J. 1991: Back-arc basins. In: Floyd P.A. (Ed.): Oceanic basalts. *Blackie*, Glasgow, 219–263.

Soldatos T. & Christofides G. 1986: Rb–Sr geochronology and origin of the Elatia Pluton, Central Rhodope, North Greece. *Geologica Balcanica* 16, 15–23.

Shervais J.W. 1982: Ti–V plots and the petrogenesis of modern ophiolitic lavas. *Earth and Planetary Science Letters* 57, 101–118.

Stampfli G.M. 2000: Tethyan oceans. In: Bozkurt E., Winchester J.A. & Piper J.D.A. (Eds.): Tectonics and magmatism in Turkey and surrounding region. *Geological Society London Special Publication* 173, 1–23.

Stampfli G.M. & Hochard C. 2009: Plate tectonics of the Alpine realm. In: Murphy J.B., Keppie J.D. & Hynes A.J. (Eds.): Ancient Orogens and Modern analogues. *Geological Society London Special Publication* 327, 89–111. https://doi.org/10.1144/SP327.6

Sun S.S. & McDonough W.F. 1989: Chemical and isotopic systematics of ocean basalts: implications for mantle composition and processes. In: Saunders A.D. & Norry M.J. (Eds.): Magmatism in Ocean Basins. *Geological Society London Special Publication* 42, 313–345.

Tatsumi Y. & Eggins R. 1995: Subduction zone magmatism. *Blackwell Science*, Cambridge, Massachusetts, 1–211.

Taylor B. & Martinez F. 2003: Back-arc basin basalt systematics. *Earth and Planetary Science Letters* 210, 481–497. https://doi.org/10.1016/S0012-821X(03)00167-5

von Quadt A. & Peytcheva I. 2005: The southern extension of Srednogorie type Upper Cretaceous magmatism in Rila-western Rhodopes: constraints from isotope-geochronological and geochemical data. In: *Proceedings of the Annual International Conference 80th Anniversary of the Bulgarian Geological Society*, 113–116.

Whitney D.L. & Evans B.W. 2010: Abbreviations for names of rock-forming minerals. *American Mineralogist* 95, 185–187. https://doi.org/10.2138/am.2010.3371

Winchester J.A. & Floyd P.A. 1977: Geochemical discrimination of different magma series and their differentiation products using immobile elements. *Chemical Geology* 20, 325–343.

Wood D.A. 1980: The application of a Th–Hf–Ta diagram to problems of tectonomagmatic classification and to establishing the nature of crustal contamination of basaltic lavas of the British Tertiary volcanic province. *Earth and Planetary Science Letters* 50, 11–30.

Zagorchev I., Moorbath S. & Lilov P. 1987: Radiogeochronological data on the Alpine igneous activity in the western part of the Rhodope Massif. *Geologica Balcanica* 17, 59–71.

Zagorchev I.S. 1998: Pre-Priabonian Paleogene formations in southwest Bulgaria and northern Greece: stratigraphy and tectonic implications. *Geological Magazine* 135, 101–119.

Electronic supplementary material is available online:
Supplementary Table S1 at http://geologicacarpathica.com/data/files/supplements/GC-74-1-Bonev_TableS1.docx
Supplementary Table S2 at http://geologicacarpathica.com/data/files/supplements/GC-74-1-Bonev_TableS2.docx
Supplementary Table S3 at http://geologicacarpathica.com/data/files/supplements/GC-74-1-Bonev_TableS3.docx

Supplement

Table S1: Summary of the petrography and mineralogy of the studied meta-mafic rock samples. Mineral abbreviations after Whitney & Evans (2010).

Sample	Rock type	Texture	Mineralogical composition/association	Remarks	Location
R1	garnet amphibolite	porphyroblastic	Amp, Qz, Pl, Ep, Fe-Ti oxide, Ttn, Grt	Qz and Ep inclusions in Grt	N41°26'52.20" E25°39'02.02"
R2	banded amphibolite	schistose	Amp, Pl, Ep, Ttn	Ep replaces Amp	N41°21'09.18" E25°39'12.86"
R3	massive amphibolite	granoblastic	Pl, Amp, Qz, Ep, Ttn, Zrn	Ep replaces Amp and Pl	N41°19'39.20" E25°38'08.18"
R4	massive amphibolite	granoblastic	Amp, Pl, Fe-Ti oxide, Qz, Rt, Zrn	preserved igneous grain shape	N41°18'21.57" E25°19'38.21"
R5	garnet amphibolite	porphyroblastic	Amp, Pl, Qz, Fe-Ti oxide, Ep, Grt, Ap, Chl, Cal	Chl replaces Amp, Pl altered to sossourite, secondary Cal	N41°26'00.75" E25°42'26.21"
R6	banded amphibolite	granoblastic	Amp, Pl, Ep, Fe-Ti oxide, Zrn	Ep replaces Amp	N41°22'11.42" E26°03'44.85"
R7	banded amphibolite	schistose	Amp, Pl, Ep, Qz, Ttn	Ep replaces Amp	N41°21'23.79" E26°05'49.47"
R8	massive amphibolite	schistose	Amp, Pl, Ep, Ttn, Mt, Zrn	Pl contains Ep and Ttn inclusions, late Mt	N41°23'24.76" E26°01'35.10"
R9	garnet amphibolite	porphyroblastic	Amp, Ep, Qz, Grt, Fe-Ti oxide	Ep replaces Pl, Qz and Ep inclusions in Grt	N41°24'53.58" E25°53'17.29"
R10	dunite	mesh	Ol, Fe-Ti oxide, Chr, Spl	Serpentine replaces Ol, Chr nodules	N41°18'11.83" E25°42'45.14"
R11	massive amphibolite	granoblastic	Amp, Ep, Qz, Fe-Ti oxide	Ep replaces Amp	N41°23'39.92" E25°35'25.37"
R12	garnet amphibolite	porphyroblastic	Amp, Pl, Fe-Ti oxide, Qz, Rt, Ilm, Ep, Grt	Qz, Ep and Rt inclusions in Grt	N41°20'07.46" E25°35'38.06"
R13	massive amphibolite	granoblastic	Amp, Pl, Qz, Ep, Ttn, Rt, Zrn	Ep replaces Amp	N41°19'25.31" E25°40'50.73"
R14	garnet amphibolite	porphyroblastic	Amp, Qz, Pl, Ep, Fe-Ti oxide, Ttn, Grt	Qz and Ep inclusions in Grt	N41°25'12.06" E25°38'35.48"
R15	garnet amphibolite	porphyroblastic	Amp, Pl, Fe-Ti oxide, Qz, Ttn, Ep, Grt	Mt inclusions in Grt	N41°24'39.00" E25°35'23.62"
R16	massive amphibolite	granoblastic	Amp, Pl, Ep, Fe-Ti oxide, Zrn	Ep replaces Amp	N41°21'25.87" E26°11'35.51"
R17	garnet amphibolite	porphyroblastic	Amp, Pl, Qz, Fe-Ti oxide, Grt, Ttn, Ep	Pl, Qz, Mt, Chl, Ep inclusions in Grt	N41°17'30.01" E26°05'26.09"
R18	massive amphibolite	granoblastic	Amp, Pl, Qz, Fe-Ti oxide, Ep, Ttn, Ms	Ep replaces Pl, Ap inclusions in Pl	N41°19'02.90" E26°28'05.99"

Table S2: Representative mineral compositions in some of the studied meta-mafic rocks.

Sample	**R9**	**R1**	**R17**	**R17**	**R 16**	**R1**	**R6**	**R17**
Mineral	**grt**	**grt**	**grt**	**pl**	**ep**	**amph**	**amph**	**amph**
Rock type	**grt-amph**	**grt-amph**	**grt-amph**	**grt-amph**	**amph**	**grt-amph**	**grt-amph**	**grt-amph**
SiO_2	37.20	37.63	37.61	65.10	38.42	43.24	47.76	43.44
TiO_2	0.14	0.11	0.04	0.007	0.14	0.61	0.51	1.03
Al_2O_3	21.03	21.24	21.41	22.03	28.27	12.07	10.52	13.77
Cr_2O_3	0.05	0.01	0.00	–	0.06	0.01	0.13	0.01
Fe_2O_3	0.66	1.38	1.90	0.01	7.09	6.74	4.23	7.61
FeO	27.1	24.54	26.36	–	–	11.35	5.96	7.88
MnO	1.11	3.47	1.49	–	–	0.21	0.17	0.18
Mn_2O_3	–	–	–	–	0.13	–	–	–
MgO	2.33	2.70	4.04	0.01	0.10	10.11	14.85	10.74
CaO	9.55	10.02	7.70	2.69	23.87	11.27	11.30	9.72
Na_2O	–	–	–	9.94	–	1.92	1.86	2.44
K_2O	–	–	–	0.07	–	0.32	0.27	0.67
H_2O	–	–	–	–	1.93	2.02	2.10	2.05
Total	99.19	101.14	100.58	99.85	100.01	99.87	99.65	99.55
Si	2.97	2.96	2.95	2.86	2.98	6.407	6.816	6.351
Ti	0.009	0.006	0.002	0.000	0.008	0.068	0.054	0.113
Al^{IV}	0.023	0.034	0.048	1.143	0.017	1.593	1.184	1.649
Al^{VI}	1.959	1.938	1.930	0	2.569	0.514	0.586	0.723
Cr	0.003	0.001	0	–	0.004	0.001	0.015	0.001
Fe^{3+}	0.042	0.082	0.112	0.001	0.414	0.752	0.454	0.837
Fe^{2+}	1.813	1.617	1.735	–	–	1.406	0.711	0.964
Mn^{2+}	0.075	0.232	0.099	–	–	0.027	0.020	0.022
Mn^{3+}	–	–	–	–	0.007	–	–	–
Mg	0.278	0.276	0.471	0.000	0.011	2.232	3.160	2.34
Ca	0.818	0.846	0.648	0.126	1.985	1.789	1.728	1.523
Na	–	–	–	0.848	–	0.552	0.515	0.692
K	–	–	–	0.004	–	0.06	0.05	0.125
OH	–	–	–	–	1	2	2	2
Py	9.331	9.307	17.376	–	–			
Alm	60.721	54.404	58.735	–	–			
Sp	2.523	7.802	3.357	–	–			
And	2.085	4.044	5.490	–	–			
Uv	0.168	0.052	0.029	–	–			
Gro	25.169	24.388	16.438	–	–			
xMg	0.133	0.145	0.211	–	–	0.614	0.816	0.708
Ab	–	–	–	86.637	–			
An	–	–	–	12.947	–			
Or	–	–	–	0.415	–			

Structural formula based on 23, 24 and 32 oxygen atoms respectively for amphiboles, garnets and feldspars.
Abbreviations: grt – garnet; grt-amph – garnet-amphibolite; amph – massive/banded amphibolite; pl – plagioclase; ep – epidote, amph – amphibole.

Table S3: Chemical analyses of major (wt. %), trace and rare earth elements (ppm) of meta-mafic rocks from the eastern Rhodope Massif. Location of the samples in Fig. 1.

Sample	**R1**	**R2**	**R3**	**R4**	**R5**	**R6**	**R7**	**R8**	**R9**
Rock type	**grt-amph**	**amph**	**amph**	**amph**	**grt-amph**	**amph**	**amph**	**amph**	**grt-amph**
Group	**High-Ti**	**High-Ti**	**High-Ti**	**High-Ti**	**High-Ti**	**Low-Ti**	**Low-Ti**	**High-Ti**	**High-Ti**
SiO_2	49.42	51.55	59.22	47.36	42.93	52.46	46.52	46.92	50.55
TiO_2	1.81	1.24	1.04	1.82	3.76	0.72	0.58	2.52	1.61
Al_2O_3	12.97	14.83	16.29	13.86	13.04	15.42	21.59	13.13	15.43
Fe_2O_3	13.65	9.88	5.82	14.17	18.49	9.48	6.23	15.57	10.51
MnO	0.18	0.16	0.11	0.21	0.29	0.16	0.11	0.20	0.16
MgO	6.94	7.15	4.20	7.59	5.86	4.73	5.70	5.32	6.32
CaO	9.76	8.84	5.84	10.32	6.91	11.79	13.61	10.19	9.02
Na_2O	2.90	4.18	6.06	2.77	1.63	1.95	1.65	2.72	3.43
K_2O	0.32	0.44	0.32	0.36	0.38	0.67	0.51	0.63	0.22
P_2O_5	0.16	0.11	0.21	0.17	0.10	0.19	0.03	0.27	0.17
Cr_2O_3	0.02	0.03	0.02	0.03	0.01	0.03	0.05	0.01	0.05
NiO	0.01	0.01	n.d.	0.01	n.d.	0.01	0.01	n.d.	0.02
LOI	1.55	1.11	0.72	1.04	6.13	1.66	2.55	1.67	1.69
Total	99.67	99.52	99.84	99.71	99.54	99.25	99.13	99.14	99.18
Nb	8	6	5	8	8	5.8	1.5	8.2	10.1
Zr	106	93	147	100	75	116	18	196	115
Y	36	29	31	38	30	20.9	6.7	59.1	26.5
Ta	1.40	1.18	2.04	1.30	0.79	3.71	4.04	2.18	3.34
Rb	7	5	5	7	14	14.6	15.2	8.4	8.3
Sr	92	167	180	120	99	550	216	92	169
Ba	<9<	36	135	20	46	142	83	72	27
U	2	3	3	2	2	<2<	<2<	<2<	<2<
Th	4	5	6	4	4	8	<2<	3	3
Pb	21	12	8	14	6	22	6	11	6
Hf	5	4	5	4	4	3.24	0.33	5.36	3.36
Sc	52	40	22	50	108	n.a.	n.a.	n.a.	n.a.
Cr	111	192	82	201	55	169	315	52	357
V	409	277	167	421	819	232	217	425	240
Ni	58	47	35	76	11	58	88	39	173
Ga	20	19	14	19	23	19	16	22	17
Zn	115	60	31	111	101	165	149	237	131
Cu	56	22	12	32	48	n.a.	n.a.	n.a.	n.a.
Co	79	63	58	74	79	n.a.	n.a.	n.a.	n.a.
La	3.98	4.88	12.23	5.62	2.54	19.90	0.61	9.61	7.41
Ce	11.69	13.67	27.78	13.29	8.32	36.25	1.64	23.84	18.02
Pr	1.92	1.85	3.53	2.24	1.45	4.74	0.26	4.01	2.46
Nd	11.51	10.06	16.11	13.23	9.20	22.36	1.80	23.39	14.46
Sm	4.23	2.65	3.93	4.02	3.47	4.32	0.53	7.62	4.20
Eu	1.39	1.09	1.27	1.44	1.81	1.20	0.45	2.27	1.24
Gd	6.66	3.00	4.19	6.87	5.22	4.28	1.04	9.07	4.64
Tb	1.07	0.60	0.74	1.40	0.90	0.69	0.26	1.75	0.73
Dy	8.02	4.25	5.36	8.92	6.34	4.88	1.65	12.12	5.29
Ho	1.70	0.85	0.85	1.94	1.51	0.84	0.32	2.54	1.26
Er	5.35	2.49	2.92	5.78	4.38	3.01	1.39	7.22	3.38
Tm	0.82	0.38	0.39	0.89	0.63	0.33	0.14	1.09	0.47
Yb	5.21	2.51	2.96	5.74	3.98	2.09	1.01	7.76	3.37
Lu	0.69	0.39	0.44	0.62	0.58	0.39	0.21	1.06	0.43

Major and trace elements determined by XRF; REE and Ta analyzed by LA-ICP-MS. n.a.= not analyzed; n.d.= not determined.
Abbreviations: grt-amph – garnet-amphibolite; amph – massive/banded amphibolite.

Table S3 (continued)

Sample	R10	R11	R12	R13	R14	R15	R16	R17	R18
Rock type	d	amph	grt-amph	amph	grt-amph	amph	amph	grt-amph	amph
Group	Low-Ti	High-Ti	High-Ti	Low-Ti	High-Ti	High-Ti	Low-Ti	Low-Ti	Low-Ti
SiO_2	38.98	47.65	49.07	50.72	48.64	53.35	46.81	58.96	55.26
TiO_2	0.03	1.46	1.81	0.26	1.76	1.47	0.42	0.43	0.26
Al_2O_3	1.32	15.18	13.61	15.62	13.14	16.76	15.32	12.14	15.61
Fe_2O_3	8.01	11.33	14.35	4.78	13.84	9.29	9.68	10.89	8.24
MnO	0.11	0.23	0.22	0.13	0.23	0.21	0.17	0.31	0.16
MgO	37.32	5.90	6.18	10.69	6.47	4.72	9.95	6.23	6.61
CaO	0.05	14.61	9.02	13.06	10.31	8.04	14.40	6.26	10.17
Na_2O	n.d	1.04	3.84	2.72	2.72	3.92	1.19	2.69	1.94
K_2O	0.01	0.27	0.22	0.26	0.32	0.80	0.27	0.56	0.23
P_2O_5	0.01	0.14	0.16	0.01	0.15	0.27	0.02	0.18	0.03
Cr_2O_3	0.42	0.05	0.02	0.08	0.02	0.01	0.08	n.d.	0.01
NiO	0.25	0.02	0.01	0.01	0.01	0.01	0.01	n.d.	n.d.
LOI	12.56	1.58	0.84	1.77	0.79	1.38	2.06	1.16	1.81
Total	99.07	99.45	99.35	100.10	98.38	100.22	100.37	99.81	100.33
Nb	10	4	9	0.20	8	6	3	7	3
Zr	22	98	111	6	99	160	12	22	30
Y	7	32	36	8	36	43	12	18	13
Ta	n.d	n.d	n.d.	0.04	n.d.	1.37	1.24	2.48	1.76
Rb	4	7	6	3	7	16	7	12	4
Sr	3	283	105	392	108	297	78	59	100
Ba	25	<9<	<9<	57	9	529	<9<	45	28
U	<2<	2	<2<	3	<2<	2	3	2	<2<
Th	<2<	5	<2<	0.08	3	4	4	3	3
Pb	5	6	3	2	<2<	9	24	20	19
Hf	<1<	3	7	0.24	3	6	3	4	3
Sc	36	29	58	37	58	29	27	42	32
Cr	2756	304	153	483	138	72	472	27	50
V	50	291	433	140	430	201	301	299	226
Ni	1401	139	68	90	54	48	70	9	23
Ga	6	20	21	11	21	20	13	12	14
Zn	39	69	114	34	126	83	64	87	61
Cu	<2<	106	69	9	67	45	82	9	76
Co	142	46	50	35	44	62	72	88	88
La	<4<	8	7	0.40	5	11.26	0.86	1.33	1.67
Ce	<3<	21	18	1.08	21	28.48	0.87	3.25	3.61
Pr	n.d.	n.d.	n.d.	0.22	n.d.	4.52	0.30	0.48	0.42
Nd	<4<	13	8	1.33	14	21.73	2.05	2.46	2.30
Sm	n.d.	n.d.	n.d.	0.50	n.d.	6.37	0.71	0.99	0.86
Eu	n.d.	n.d.	n.d.	0.46	n.d.	2.02	0.34	0.44	0.34
Gd	n.d.	n.d.	n.d.	1.28	n.d.	8.58	1.11	1.80	1.50
Tb	n.d.	n.d.	n.d.	0.23	n.d.	1.33	0.18	0.42	0.27
Dy	n.d.	n.d.	n.d.	1.61	n.d.	8.99	1.34	3.08	1.84
Ho	n.d.	n.d.	n.d.	0.32	n.d.	2.08	0.31	0.62	0.38
Er	n.d.	n.d.	n.d.	0.89	n.d.	5.64	1.06	2.02	1.03
Tm	n.d.	n.d.	n.d.	0.09	n.d.	0.85	0.12	0.25	0.22
Yb	n.d.	n.d.	n.d.	0.99	n.d.	5.32	1.06	2.07	1.27
Lu	n.d.	n.d.	n.d.	0.17	n.d.	0.80	0.10	0.26	0.20

Major and trace elements determined by XRF; REE and Ta analyzed by LA-ICP-MS. n.a.= not analyzed; n.d.= not determined.
Abbreviations: d, dunite; grt-amph, garnet-amphibolite; amph, massive/banded amphibolite.